Slit3 Fragments Orchestrate Neurovascular Expansion and Thermogenesis in Brown Adipose Tissue

Tamires Duarte Afonso Serdan[1], Benjamin Frank[1,*], Heidi Cervantes[1,*], Akhil Gargey[1,] Qiyu Tian[1], Daniel Hope[1], Chan Hee J. Choi[2], Anne Hoffmann[3], Paul Cohen[2], Matthias Blüher[3,4], Halil Aydin[1], Gary J Schwartz[5], Farnaz Shamsi[1,6]

[1]Department of Molecular Pathobiology, College of Dentistry, New York University, New York, NY, USA.

[2]Laboratory of Molecular Metabolism, The Rockefeller University, New York, NY, USA.

[3]Helmholtz Institute for Metabolic, Obesity and Vascular Research (HI-MAG) of the Helmholtz Center Munich at the University of Leipzig and University Hospital Leipzig, Leipzig, 04103, Germany.

[4]Medical Department III–Endocrinology, Nephrology, Rheumatology, University of Leipzig Medical Center, Leipzig 04103, Germany.

[5]Departments of Medicine and Neuroscience, Fleischer Institute for Diabetes and Metabolism, Albert Einstein College of Medicine, Bronx, NY 10461, USA.

[6]Departments of Cell Biology and Medicine, Grossman School of Medicine, New York University, New York, NY, USA. Email: fs2451@nyu.edu

* These authors contributed equally

Abstract

Brown adipose tissue (BAT) is an evolutionary innovation that enables placental mammals to regulate body temperature through adaptive thermogenesis. Brown adipocytes are embedded within an intricate network of blood vessels and sympathetic nerves that support their development and thermogenic function. Cold exposure activates BAT thermogenesis through the coordinated induction of brown adipogenesis, angiogenesis, and sympathetic innervation. However, how these distinct processes are coordinated remains unclear. Here, we show that fragments of Slit guidance ligand 3 (Slit3) drive crosstalk among adipocyte progenitors, endothelial cells, and sympathetic nerves. We demonstrate that adipocyte progenitors secrete Slit3, which regulates both angiogenesis and sympathetic innervation in BAT and is essential for BAT thermogenesis in vivo. Proteolytic cleavage of Slit3 generates secreted Slit3-N and Slit3-C fragments, which bind distinct receptors to stimulate angiogenesis and sympathetic innervation, respectively. We identify Plxna1 as a previously unrecognized receptor for Slit3-C and show that it is essential for sympathetic innervation and cold-induced neurite expansion in BAT. Moreover, we introduce bone morphogenetic protein 1 (Bmp1) as the first Slit protease identified in vertebrates. In summary, this work establishes a mechanistic framework for the coordinated regulation of sympathetic innervation and angiogenesis to enhance thermogenic function. The co-regulation of neurovascular expansion by distinct Slit3 fragments offers a bifurcated yet harmonized mechanism to ensure a synchronized BAT response to environmental challenges. Finally, this study provides the first evidence that adipocyte progenitors regulate tissue innervation, revealing a previously unrecognized dimension of cellular interaction within adipose tissue.

Main

The regulation of body temperature, thermoregulation, is a fundamental homeostatic process in endothermic animals. Preserving a stable internal temperature ensures the efficiency and fidelity of all cellular reactions and is essential for survival. Brown adipose tissue (BAT) is a specialized type of adipose tissue that is primarily responsible for regulating body temperature through adaptive thermogenesis. Brown adipocytes oxidize substrates and generate heat to maintain euthermia in a cold environment[1].

Brown adipocytes are intricately embedded in a dense network of capillaries and sympathetic nerves. The high thermogenic activity of BAT requires a high rate of blood perfusion to supply O_2 and substrates. The sympathetic nerves also play a key role in stimulating BAT thermogenesis by releasing norepinephrine in the tissue. Norepinephrine activates adrenergic signaling in thermogenic adipocytes, resulting in enhanced thermogenesis and lipolysis[2]. Chronic cold exposure increases BAT mass by *de novo* recruitment of brown adipocytes, as well as by expanding the network of blood vessels and sympathetic nerves in the tissue. This coordinated expansion of the BAT ensures its continuous responsiveness to hormonal and neuronal stimuli and is essential for enhanced thermogenesis in cold[3,4]. However, how these distinct processes are spatiotemporally coordinated remains unclear. Furthermore, while significant progress has been made in understanding the molecular mechanisms of thermogenic activation in adipocytes, the equally crucial process of remodeling the thermogenic adipose niche remains less understood.

Cell–cell communication is vital for organismal development and function. Ligand-receptor interactions allow cells in complex tissues to coordinate their functions during development, homeostasis, and remodeling. To understand the mechanisms through which different cell types in BAT communicate and synchronize their response to cold to collectively enhance thermogenesis, we recently used single-cell transcriptomic data[5] to construct a network of ligand-receptor interactions in BAT[6]. That study highlighted the central role of adipocyte progenitors, not

75 merely as the source of adipocytes, but also as key communicators and versatile players in the
76 adipose tissue microenvironment. These progenitors have been shown to contribute to a variety
77 of processes, including extracellular matrix remodeling, immune modulation, and angiogenesis[7].
78 Here, we demonstrate that Slit3 is a critical regulator of BAT neurovascular development
79 and function. We show that Slit3 mediates crosstalk among adipocyte progenitors, endothelial
80 cells, and sympathetic nerves, regulating both angiogenesis and innervation. Using BAT- and
81 adipocyte progenitor-specific loss of function models, we show that the loss of Slit3 disrupts both
82 angiogenesis and sympathetic innervation, ultimately blunting cold-induced BAT thermogenesis.
83 We identify BMP1 as the protease responsible for Slit3 cleavage and reveal that the resulting
84 fragments activate distinct pathways: Slit3-N promotes angiogenesis, while Slit3-C, through its
85 newly identified receptor Plxna1, drives sympathetic innervation. This pathway demonstrates a
86 sophisticated level of intercellular coordination whereby a single factor simultaneously drives
87 these two distinct processes essential for thermogenic activation.

88 **Results**

89 **Identification of Slit3-Robo4 signaling axis in BAT**

90 Intercellular communication plays a critical role in coordinating tissue adaptation to
91 external challenges. To define the role of intercellular crosstalk in cold-induced BAT
92 thermogenesis, we previously used single-cell transcriptomic data to build a network of ligand-
93 receptor interactions involved in the cold-induced remodeling of BAT[6]. This analysis revealed the
94 significance of adipocyte progenitors as the major communication hub in the adipose niche[6]. This
95 prompted us to search for ligands secreted from adipocyte progenitors that might mediate the
96 crosstalk between adipocyte progenitors and their niche. Ligand-receptor analysis of BAT
97 identified a new crosstalk axis in BAT involving the axon guidance molecule Slit3 and its cognate
98 receptor, Robo4. In BAT, Slit3 is predominantly expressed in Pdgfra+ and Trpv1+ adipocyte
99 progenitors, as well as in vascular smooth muscle cells, while its receptor, Robo4, is exclusively

100 expressed in vascular and lymphatic endothelial cells (Figure 1a). To validate these findings, we
101 separated the stromal vascular and adipocyte fractions of mouse BAT, sorted distinct cell
102 populations, and measured Slit3 expression. This analysis confirmed that adipocyte progenitors
103 are the primary source of Slit3 in BAT under both basal and cold-acclimated conditions (Figure
104 1b and Supplementary Figure 1a-d), whereas Robo4 is exclusively expressed in endothelial cells
105 (Supplementary Figure 1e). To examine Slit3 protein expression in BAT and its regulation by
106 environmental temperature, we performed Western blot analysis on BAT from mice housed at
107 different temperatures. Slit3-FL levels were elevated in BAT of mice exposed to cold for 2 days
108 compared to those maintained at room temperature (Figure 1c-d). These findings indicates that
109 cold exposure enhances Slit3 protein levels in BAT.

110 A previous study reported that Slit3 is secreted from macrophages in white adipose tissue
111 (WAT)[8]. However, our unbiased scRNA-seq data, along with targeted expression analysis in
112 isolated macrophages, did not detect any Slit3 expression in BAT macrophages (Figure 1a-b).
113 Analysis of scRNA-seq datasets from mouse inguinal white adipose tissue (ingWAT) and
114 perigonadal white adipose tissue (pgWAT), as well as human WAT[9], revealed Slit3 expression in
115 adipocyte progenitors, mesothelial cells, and mural cells (vascular smooth muscle cells and
116 pericytes) (Supplementary Figure 2a-d), but no expression in macrophages in either mouse or
117 human WAT (Supplementary Figure 2a-d). Collectively, these findings suggest that adipocyte
118 progenitors, rather than macrophages, are the primary source of Slit3 in adipose tissue.

119 To assess the temporal pattern of Slit3 expression during adipogenesis, we measured
120 SLIT3 protein levels in a mouse brown adipocyte progenitor cell line at multiple time points
121 throughout in vitro adipogenic differentiation. SLIT3 protein levels sharply decreased by days 4
122 and 8 of differentiation, in contrast to the increasing UCP1 expression (Supplementary Figure 2e).
123 These results indicate that SLIT3 expression is significantly higher in adipocyte progenitors than
124 in mature adipocytes, where SLIT3 protein levels were minimal.

125 **Axon Guidance Molecule Slit3 is essential for BAT thermogenesis.**

126 To investigate Slit3 function in BAT, we used AAV-mediated shRNA delivery to knock
127 down Slit3 expression in all Slit3-expressing cell types specifically in BAT. We confirmed a
128 significant reduction in Slit3 transcript and protein levels in BAT, but not in WAT, of mice receiving
129 Slit3 shRNAs (Supplementary Figure 3a-d). Mice lacking Slit3 expression in BAT exhibited severe
130 impairments in cold-induced thermogenesis, maintaining lower core body temperature (Figure 1e)
131 and BAT temperature (Supplementary Figure 3e) during cold exposure.

132 After seven days of cold exposure, analysis of BAT revealed pronounced whitening and
133 increased lipid accumulation (Figure 1f), along with reduced expression of uncoupling protein 1
134 (Ucp1) (Figure 1g-h) and other thermogenic and mitochondrial genes in Slit3 knockdown mice
135 (Figure 1i). Furthermore, Slit3 loss resulted in a marked reduction in mitochondrial electron
136 transport chain complex levels (Figure 1j-k). Mice lacking Slit3 expression in BAT exhibited a
137 similar reduction in Ucp1 transcript and protein levels at room temperature. However, the
138 expression of other thermogenic and mitochondrial genes remained largely unchanged under
139 these conditions (Supplementary Figure 4a-c).

140 Consistent with histological and molecular analyses, Slit3 loss in BAT significantly reduced
141 energy expenditure, oxygen consumption, and CO_2 production in mice housed at 5°C (Figure 1l-
142 m, Supplementary Figure 5). Importantly, these metabolic alterations occurred without changes
143 in body weight, body composition, respiratory exchange ratio, food intake, or locomotor activity
144 (Supplementary Figure 5). Together, these findings establish Slit3 as a critical regulator of cold-
145 induced BAT thermogenesis and energy expenditure.

146 **Loss of Slit3 impairs cold-induced angiogenesis and sympathetic innervation in BAT.**

147 To investigate how the loss of Slit3 impairs cold-induced BAT thermogenesis, we first
148 examined the cell-autonomous effects of Slit3 on adipocytes. We treated in vitro-differentiated
149 brown adipocytes with recombinant Slit3-N and Slit3-C proteins. qPCR and immunoblot analyses
150 showed no changes in the expression of Ucp1 or other thermogenic genes in adipocytes treated

151 with recombinant Slit3 fragments (Supplementary Figure 6a-b). These results led us to
152 hypothesize that Slit3 loss impairs BAT thermogenesis by disrupting the brown adipocyte niche

153 The expansion of BAT neurovasculature is essential for cold adaptation and enhanced
154 thermogenesis in the cold[3,4]. Chronic cold exposure significantly increases the density of
155 parenchymal sympathetic neurites and capillary blood vessels in BAT (Supplementary Figure 6c-
156 f). To investigate putative mechanism(s) underlying impaired BAT thermogenesis in Slit3-deficient
157 mice, we assessed vascularization and sympathetic innervation in BAT from Slit3 knockdown or
158 control mice after seven days of cold exposure (5 °C). Analysis of BAT vasculature revealed that
159 Slit3 knockdown significantly impaired angiogenesis, as indicated by a reduction in capillary
160 density (Figure 2a-b) and a decrease in endothelial-specific transcript expression (Figure 2c).

161 The loss of Slit3 also resulted in a dramatic reduction in the density of Tyrosine
162 Hydroxylase (TH)-expressing neurites in BAT (Figure 2d-e). To assess the architecture and
163 density of sympathetic innervation, we used the Adipo-Clear protocol[10] to stain TH-expressing
164 sympathetic nerves in BAT, followed by Lightsheet microscopy. 3D volumetric images of TH-
165 positive nerves revealed a marked decline in parenchymal innervation in Slit3-deficient BAT
166 (Figure 2f). Furthermore, total TH protein levels in BAT were significantly reduced in the absence
167 of Slit3 (Figure 2g-h). Notably, even when animals were housed at room temperature, loss of Slit3
168 led to a decrease in both capillary density and sympathetic innervation in BAT (Supplementary
169 Figure 7a-d). However, housing at cold temperatures further exacerbated these defects. These
170 findings underscore the crucial role of Slit3 in the development and expansion of the
171 neurovascular network in BAT, especially during adaptation to cold environment.

172 **Adipocyte progenitor-derived Slit3 is essential for cold-induced neurovascular expansion**
173 **in BAT.**

174 To further confirm that adipocyte progenitors are the primary source of Slit3 and that
175 progenitor-derived Slit3 is essential for cold-induced neurovascular expansion and BAT

176 thermogenesis, we specifically deleted Slit3 in Pdgfra-expressing cells by crossing Slit3 floxed
177 mice[11] with an inducible Pdgfra-cre strain[12] (Pdgfra-creERT2;Slit3$^{flox/flox}$ or Slit3$^{i\Delta APC}$). Western
178 blotting showed a complete loss of Slit3 protein in BAT and a marked reduction in WAT of Slit3$^{i\Delta APC}$
179 mice (Figure 3a-c and supplementary Figure 8a-b). Consistent with the observed phenotypes in
180 BAT-specific Slit3 knockdown mice, both male and female Slit3$^{i\Delta APC}$ mice exhibited significant
181 impairments in BAT thermogenesis and were cold intolerant (Figure 3d-e), highlighting the
182 essential role of adipocyte progenitor-derived Slit3 in cold adaptation. Similar to our findings with
183 Slit3 knockdown in BAT, Slit3$^{i\Delta APC}$ mice exposed to cold showed a significant reduction in both
184 sympathetic neurite and capillary density in BAT (Figure f-i). Together, these results confirm that
185 Pdgfra-expressing adipocyte progenitors are the primary source of Slit3 in BAT, and that the loss
186 of progenitor-derived Slit3 disrupts cold-induced neurovascular expansion, leading to impaired
187 thermogenic activation.

188 **Bmp1-mediated proteolytic cleavage of Slit3 generates two secreted ligands.**

189 Members of the Slit family are proteolytically cleaved into a large N-terminal and a shorter
190 C-terminal fragment[13]. However, the functional implications of Slit cleavage and the distinct roles
191 played by the full-length protein and its fragments remain unclear. Additionally, the Slit proteases
192 in vertebrates have not been identified.

193 To investigate whether Slit3 is cleaved in adipocyte progenitors, we overexpressed an N-
194 and C-terminal tagged wild-type Slit3 (SNAP-Slit3-HaloTag) as well as an uncleavable Slit3
195 variant (SNAP-Slit3UC-HaloTag) in a brown adipocyte progenitor cell line (Figure 4a). Using
196 antibodies against HaloTag and SNAP-tag, we detected the full-length Slit3 protein (Slit3-FL) in
197 the total cell lysates of cells overexpressing either the wild-type or uncleavable Slit3 constructs
198 (Figure 4b-c). The HaloTag antibody detected two bands in the conditioned media of cells
199 overexpressing SNAP-Slit3-HaloTag: a ~200 kDa band corresponding to the tagged full-length
200 Slit3 and a ~60 kDa band matching the expected size of the tagged Slit3C-terminal fragment

201 (Slit3-C). In contrast, the media from cells expressing the uncleavable Slit3 only contained the
202 Slit3-FL (Figure 4b). Similarly, the SNAP-tag antibody detected both the Slit3-FL and a ~150 kDa
203 band corresponding to the tagged Slit3 N-terminal fragment (Slit3-N) in the media of cells
204 overexpressing SNAP-Slit3-HaloTag (Figure 4c). A minor amount of Slit3-N, but not Slit3-C, was
205 also detected in the total cell lysates, which contain membrane and membrane-associated
206 proteins (Figure 4c). This finding is consistent with previous reports suggesting that the N-terminal
207 fragment of Slits may remain associated with the plasma membrane, while the C-terminal
208 fragment is more diffusible[13]. Collectively, these data indicate that Slit3 cleavage in adipocyte
209 progenitors generates Slit3-N and Slit3-C fragments, and that Slit3-FL, Slit3-N, and Slit3-C
210 fragments are secreted factors.

211 Moreover, analysis of a proteomics dataset of the adipocyte secretome showed the
212 presence of Slit3 in the conditioned media of *in vitro* differentiated adipocytes derived from mouse
213 visceral (Visc), subcutaneous inguinal white (SubQ), and interscapular BAT[14] (Figure 4d). Slit3
214 was significantly more abundant in the conditioned media of brown and subcutaneous white
215 adipocytes than visceral white adipocytes. These results indicated that Slit3 is secreted by various
216 adipocyte types *in vitro*, with the highest abundance observed in the secretome of brown
217 adipocytes.

218 A recent study suggested a role for the metalloprotease Tolkin (Tok) in Slit proteolysis in
219 *Drosophila melanogaster*[15]. Tok is a member of the Bmp1/Tolloid family of metalloproteases. In
220 mammals, the Bmp-1/tolloid-like family includes bone morphogenetic protein-1 (Bmp1), tolloid
221 (Tld), and tolloid-like 1 and 2 (Tll1 and Tll2). Given the similarity in the cleavage sites among the
222 members of the Slit family[15], we hypothesized that the Bmp1/Tolloid proteases might be involved
223 in Slit3 cleavage. Among the members of the Bmp1/Tolloid proteases family, only Bmp1 and Tll1
224 are expressed in BAT (Figure 4e and Supplementary Figure 9). Notably, Bmp1 is abundantly
225 expressed in Pdgfra- and Trpv1-expressing adipocyte progenitors, the major cell types expressing

226 Slit3 in BAT (Figure 4e). Bmp1 lacks growth factor activity found in other BMP family members
227 and instead functions as a metalloprotease. To discern the role of Bmp1 in Slit3 proteolysis in
228 adipocyte progenitors, we used a combination of pharmacological and genetic loss of function
229 studies. We showed that the inhibition of Bmp1 activity using a small molecule inhibitor,
230 UK383,367[16], blocked Slit3 cleavage (Figure 4f). Similarly, knocking down Bmp1 using siRNAs
231 prevented Slit3 cleavage (Figure 4g). Thus, we concluded that Bmp1 is responsible for the
232 proteolytic processing of Slit3, establishing Bmp1 as the first Slit protease in vertebrates.

233 **Slit3 fragments promote angiogenesis and sympathetic innervation in BAT.**

234 To investigate the specific functions of Slit3 fragments in BAT, we generated AAV
235 constructs for adipocyte-specific overexpression of full-length Slit3 (Slit3-FL), its N-terminal
236 fragment (Slit3-N, aa 1–1116), and its C-terminal fragment (Slit3-C, aa 1117–1523) (Figure 5a).
237 Four weeks after AAV administration in the interscapular BAT, we confirmed the specific
238 expression of Slit3-FL, Slit3-N, and Slit3-C (Figure 5b–c). Overexpression of Slit3-FL and Slit3-C,
239 but not Slit3-N, enhanced sympathetic innervation in BAT, as indicated by an increased number
240 and relative area of TH-expressing sympathetic neurites (Figure 5d–f). Furthermore,
241 overexpression of all three Slit3 variants, Slit3-FL, Slit3-N, and Slit3-C, led to increased capillary
242 density in BAT (Figure 5g–h). Mice overexpressing Slit3-FL and Slit3-C, but not Slit3-N, also
243 exhibited higher TH levels in BAT (Figure 5i–q and Supplementary Figure 10). Notably, Slit3-FL
244 and Slit3-C overexpression enhanced BAT thermogenesis, as evidenced by increased Ucp1
245 expression and higher BAT temperatures under cold exposure (Figure 5k, 5n, 5q–r). These
246 findings indicate that Slit3 fragments directly promote the expansion of BAT's neurovascular
247 network, with Slit3-C primarily driving sympathetic innervation and Slit3-N inducing angiogenesis,
248 collectively contributing to enhanced thermogenic function.

249 **Plxna1 is the Slit3 receptor that mediates sympathetic innervation in BAT.**

250 Full-length and N-terminal Slit fragments bind to transmembrane Robo receptors (Robo1-4)[36],
251 while the receptor binding and bioactivity of the C-terminal fragment (Slit-C) remains less
252 characterized. The C-terminal of Slit2 has been shown to bind Plexin A1 (Plxna1)[17], but the
253 receptor(s) for Slit3-C have yet to be identified. To identify the receptors mediating Slit3 signaling
254 in BAT, we analyzed the expression of putative Slit receptors. scRNA-seq analysis of BAT
255 revealed that among the four Robo family members, only Robo4 is expressed in BAT, where it is
256 exclusively localized to vascular and lymphatic endothelial cells (Figure 1a and Supplementary
257 Figure 1e). To validate this, we co-stained BAT sections with a Robo4 antibody and Isolectin B4.
258 We found that Robo4 was specifically localized to Isolectin B4-labeled capillaries (Figure 6a).
259 Furthermore, double staining of BAT with Robo1 and TH antibodies revealed Robo1 expression
260 in TH-expressing sympathetic neurites (Figure 6b). Similarly, Plxna1 and TH were co-localized in
261 sympathetic neurites (Figure 6c).

262 Building on our finding that Slit3-C enhances sympathetic innervation (Figure 5d–f) and
263 that Plxna1 is expressed on sympathetic neurites, we hypothesized that Plxna1 serves as the
264 receptor for Slit3-C. To address this, we first assessed the ability of Plxna1 to interact with Slit3-
265 FL or Slit3-C. We co-overexpressed the extracellular region of Plxna1, C-terminally fused to a 6X
266 histidine tag, along with Slit3-FL-HaloTag or Slit3-C-HaloTag in a mouse adipocyte progenitor cell
267 line. Using a His-tag antibody, we immunoprecipitated Plxna1 and its interacting proteins. We
268 found that both Slit3-FL and Slit3-C co-immunoprecipitated with the extracellular region of Plxna1
269 (Figure 6d). These findings indicate that Plxna1 specifically interacts with the C-terminal region of
270 Slit3 (Slit3-C), which is distinct from the N-terminal region recognized by Robo receptors[18].

271 To further investigate the interaction between Plxna1 and Slit3, we used AlphaFold2
272 Multimer to model complexes involving the extracellular domain of Plxna1 and the C-terminal
273 region of Slit3. Multiple structure predictions were generated based on sequence alignments and
274 structural relaxation, with only those having average inter-protein TM (iPTM) scores >0.5 retained

275 for further analysis. Diagnostic plots were then used to assess model quality (Supplementary
276 Figure 11). The top-ranked models, shown in Figure 7e-f, reveal two distinct interaction modes: a
277 monomeric Plxna1–Slit3 complex (Figure 7e) and a dimeric Plxna1 interacting with a monomeric
278 Slit3 (Figure 7f). Figure 7g illustrates the domain organization of Plxna1, Slit3, and Sema6d—a
279 known ligand for Plxna1—with the modeled binding regions indicated by dashed lines. The
280 predicted binding interfaces of Slit3 and Sema6d on Plxna1's extracellular domains (Figure 7h)
281 suggest a direct interaction, with the Slit3 binding region in magenta, Sema6d in cyan, and a
282 shared binding region marked in yellow. The AlphaFold2 diagnostic plots (Supplementary Figure
283 11) further validate the structural integrity of the models, with Predicted Aligned Error (PAE) plots
284 for both the monomeric and dimeric complexes, along with predicted Local Distance Difference
285 Test (pLDDT) scores, demonstrating high confidence in the predicted structures.

286 We next examined whether Plxna1 functions as a receptor for Slit3-C in vivo and whether
287 it is required for Slit3-mediated sympathetic innervation. To test this, we overexpressed Slit3-C in
288 BAT with or without Plxna1 knockdown. Consistent with earlier findings (Figure 5), Slit3-FL
289 overexpression significantly enhanced sympathetic innervation in BAT (Figure 6e–f). However,
290 this effect was abolished when Plxna1 expression was knocked down. Similarly, Plxna1
291 knockdown markedly reduced the Slit3-C-induced increase in sympathetic innervation (Figure
292 6g–h). Notably, in the absence of Plxna1, Slit3-C overexpression failed to elevate BAT
293 temperature in response to cold exposure (Figure 6i). Collectively, by combining biochemical
294 assays, computational structural modeling, and in vivo studies, we provide strong and converging
295 evidence that Plxna1 is a direct and essential receptor for the C-terminal region of Slit3, required
296 for both sympathetic innervation and thermogenic activation in BAT.

297 **Plxna1 is essential for sympathetic innervation and cold-induced neurite expansion in BAT**

298 We observed a severe reduction in sympathetic innervation of BAT and cold tolerance in
299 mice receiving Plxna1 shRNAs alone (shPlxna1 group in Figure 6e-i), suggesting that Plxna1 is
300 crucial for the development and cold-induced expansion of sympathetic neurites in BAT. To

301 directly test this, we injected AAVs delivering Plxna1 shRNAs into BAT. qPCR and Western blot
302 analysis confirmed a significant reduction of Plxna1 expression in BAT (Supplementary Figure
303 12a-b). Loss of Plxna1 led a pronounced decrease in sympathetic nerve density in mice housed
304 at room temperature as well as after three and seven days of cold exposure (Figure 7a-b). This
305 was accompanied by a reduction in total TH protein levels (Figure 7c-d and Supplementary Figure
306 12c-d) in BAT, while capillary density remained unchanged (Figure 7e-f). This resulted in impaired
307 BAT thermogenesis, evidenced by reduced BAT temperature in cold conditions (Figure 7g) and
308 a downregulation of the thermogenic gene program both at room temperature and after three
309 days of cold acclimation (Figures 7h-i). Loss of Plxna1 reduced expression of GAP43, a key
310 axonal growth cone protein involved in axon outgrowth and regeneration in BAT. This was
311 reflected by a decreased $GAP43^{+}$ neurite area and a lower proportion of sympathetic neurites
312 expressing GAP43 (Figure 7j-l). Consistently, Gap43 mRNA levels were also reduced in BAT
313 following Plxna1 knockdown (Figure 7m) .These findings establish Plxna1 as a key regulator of
314 sympathetic innervation in BAT, demonstrating for the first time its essential role in both the
315 steady-state maintenance and cold-induced expansion of sympathetic neurites in BAT (Figure
316 7n).

317 **Slit3 expression is associated with adipose tissue health and inflammation in humans**

318 Lastly, to assess the significance of SLIT3 in human obesity, we measured its expression
319 in human adipose tissue biopsies in abdominal subcutaneous WAT and omental visceral WAT
320 collected from two independent cohorts of the Leipzig Obesity BioBank (LOBB). In the
321 metabolically healthy versus unhealthy obese cohort (MHUO), we found that *SLIT3* transcript
322 levels in human abdominal subcutaneous WAT were positively correlated with serum adiponectin
323 concentrations (r=546, p=0.00176, N=31) and negatively regulated with the relative number of
324 macrophages in omental visceral WAT (r=566, p<0.001, N=31) in insulin-sensitive patients
325 (Figure 8a-b), but not in insulin-resistant patients (Figure 8c-d).

326 Additionally, we examined *SLIT3* expression in the human cross-sectional cohort
327 comprised of paired samples of omental visceral and abdominal subcutaneous WAT from 1,480
328 individuals. In this cohort, we found *SLIT3* expression in omental visceral WAT negatively
329 correlated with Hemoglobin A1C (HbA1c) ($r=0.092$, $p<0.001$, $N=1447$) (Figure 8e). Additionally,
330 *SLIT3* expression in omental visceral and abdominal subcutaneous WAT was positively
331 associated with circulating level of the anti-inflammatory adipokine Omentin1 ($r=0.164$, $p<0.001$,
332 $N=675$ and $r=0.124$, $p=0.00121$, $N=675$, respectively) (Figure 8f-g). Omentin1 has been shown
333 to play important roles in glucose homeostasis, lipid metabolism, insulin resistance, and
334 diabetes[19,20]. Collectively, these data suggest that SLIT3 may regulate adipose tissue health and
335 inflammation in humans, potentially impacting insulin sensitivity.

336 **Discussion**

337 Recent advances in technical and computational methods for studying complex tissues
338 are providing a systematic understanding of how cellular crosstalk within the tissue
339 microenvironment drives development, function, and disease mechanisms. Using scRNA-seq
340 data from BAT, this study identifies Slit3 fragments as novel niche factors mediating crosstalk
341 among adipocyte progenitors, sympathetic nerves, and blood vessels. We show that loss of Slit3
342 or Plxna1 in BAT significantly impairs cold-induced neurovascular expansion and adaptive
343 thermogenesis. Our work introduces the concept that adipocyte progenitors are dynamic
344 regulators of adipose tissue remodeling, expanding the view of their role beyond adipogenesis
345 alone. We uncover new, molecularly specific enzymatic and receptor-mediated mechanisms that
346 coordinate angiogenesis and sympathetic innervation—two essential processes for maintaining
347 adipose tissue health (Figure 7n)

348 Despite the critical roles of Slit proteins in many processes, the biological activities of Slit
349 fragments and the mechanisms controlling the context-dependent outcomes of Slit signaling are
350 still largely unclear. This is in part due to the unknown identity of the Slit proteases, which

351 prevented the separation of Slit fragment activities from that of the full-length protein. Identification
352 of Slit proteases and the specific receptors for the Slit fragments are critical for understanding the
353 mechanisms that control Slit signaling during tissue development, remodeling, and regeneration.
354 In this work, we identified the metalloprotease Bmp1 as the first known vertebrate Slit protease.
355 Through a combination of pharmacological and genetic approaches, we found that Bmp1 is
356 responsible for Slit3 cleavage. This finding highlights Bmp1's role in regulating the biological
357 activities of Slit3, and potentially other Slit family members, in various contexts, including axon
358 guidance and growth, angiogenesis, inflammatory cell chemotaxis, and tumor metastasis.

359 Bmp1 is a key protease that processes several extracellular matrix proteins and growth
360 factors. It cleaves substrates such as procollagen, lysyl oxidase, and proteoglycans, which are
361 essential for tissue integrity, including in adipose tissue[21,22]. Bmp1 also modulates the activity and
362 availability of certain growth factors by processing their precursors, thereby influencing cell
363 differentiation and tissue development[23]. Notably, whole-body Bmp1 knockout mice show reduced
364 white adipose tissue mass[24]. While it's tempting to speculate that this phenotype may be partly
365 due to impaired Slit3 cleavage, Bmp1's broad substrate specificity makes it difficult to draw direct
366 conclusions from existing data.

367 Another key finding of our study is the identification of Plxna1 as the receptor for the C-
368 terminal fragment of Slit3 and its essential role in regulating sympathetic innervation in BAT.
369 Plexins are a family of single-pass transmembrane proteins that serve as receptors for
370 Semaphorin axon guidance cues. Semaphorin-Plexin signaling regulates diverse biological
371 processes, including axon guidance, angiogenesis, and immune responses[25]. In vertebrates,
372 class A Plexins (PlxnAs) typically bind Class 6 Semaphorins and, together with Neuropilin co-
373 receptors, also interact with Class 3 semaphorins[26]. Our data show that Plxna1 is required for
374 sympathetic innervation of BAT and cold-induced induction of thermogenesis gene program.
375 Importantly, loss of Plxna1 eliminates the pro-innervation effects of both Slit3-C and full-length
376 Slit3. These findings challenge the conventional view that Slit proteins exclusively signal through

377 Robo receptors and that Plexins are limited to Semaphorin signaling. Instead, we propose a
378 previously unrecognized level of crosstalk between these two distinct ligand-receptor families.
379 Because Plxna1 also mediates Semaphorin signaling, we cannot fully exclude the possibility that
380 the reduced innervation observed in Plxna1-deficient BAT reflects, in part, impaired Semaphorin
381 pathways. Future studies will be important to dissect the relative contributions of Slit3 and
382 Semaphorin signaling through Plxna1 in regulating sympathetic innervation.

383 Adipose tissues are extensively innervated by a network of sympathetic and sensory nerve
384 projections, which facilitate the transmission of information between the adipose tissue and the
385 central nervous system. It is well-established that the sympathetic innervation of adipose tissue
386 is critical for homeostatic control of its function and whole-body metabolism[27-29]. The plasticity of
387 sympathetic nerves allows for altered neuronal control and adaptation to metabolic challenges.
388 However, the mechanisms underlying the local expansion and remodeling of sympathetic neurites
389 are not well understood. Obesity disrupts norepinephrine-mediated adipocyte lipolysis[30],
390 mitochondrial biogenesis[31], and adipose tissue remodeling[32]. These impairments are attributed to
391 dysfunctional local sympathetic innervation resulting from adipose inflammation[33]. In turn, the
392 impaired sympathetic activity in obese adipose tissue may contribute to more inflammation and
393 further exacerbate adipose dysfunction[34]. Therefore, preserving the density and functionality of
394 sympathetic nerves may help safeguard adipose tissue health in obesity. To the best of our
395 knowledge, this study is the first to demonstrate that adipocyte progenitors play a regulatory role
396 in sympathetic innervation of adipose tissue depots, introducing a previously unexplored regulator
397 of adipose tissue innervation.

398 Genome-wide association studies have found genetic variants near the SLIT3 gene to be
399 associated with an increased risk of insulin resistance[35] and higher BMI[36]. Additionally, a
400 differentially methylated CpG in the SLIT3 gene in visceral adipose tissue was found to be
401 associated with the development of type 2 diabetes in obese women[37]. Genetic variants in
402 PLXNA1 gene are also associated with severe early onset obesity[38]. These independent findings

403 suggest that SLIT3 and its receptor PLXNA1 may have a role in regulating metabolism in humans.
404 Our analysis of human adipose tissue in two obesity cohorts suggest that SLIT3 signaling may
405 contribute to improved adipose tissue health, reduced inflammation, and insulin sensitivity in
406 human obesity. These findings highlight the need for further investigation into SLIT3-PLXNA1
407 signaling in the context of obesity and metabolic disease.
408

409 **Methods**

410 **Animals.** All experimental procedures involving animals were performed in compliance with all
411 relevant ethical regulations applied to the use of small rodents and with approval by the
412 Institutional Animal Care and Use Committees at New York University. C57BL/6J mice (stock no.
413 000664) were purchased from Jackson Laboratory. Pdgfra-cre;Slit3$^{flox/flox}$ or Slit3$^{i\Delta APC}$ were
414 generated by crossing Slit3 floxed mice[11] with Pdgfra-creER^{TM} [12] (JAX strains 018280). Mice
415 were maintained on a 12-h light-dark cycle at 22 °C and 50% relative humidity, with food and
416 water provided ad libitum. For experiments involving cold acclimation, mice were housed at 5°C
417 and 50% relative humidity in a controlled environmental diurnal chamber (Caron Products &
418 Services) with free access to food and water.

419 **Cold tolerance test.** For cold tolerance tests, mice were single-housed and placed at 5°C in a
420 controlled environmental diurnal chamber (Caron Products & Services). Body temperature was
421 measured with a rectal probe (Physitemp, RET3) and a reader (Physitemp, BAT-12) or using
422 RFID transponder temperature microchips implanted under the interscapular BAT area (Unified
423 Information Devices).

424 **AAV injection.** 6-8-week-old male mice were anesthetized with isoflurane and an incision was
425 made above the interscapular area to expose the underlying adipose tissue. AAV particles were

426 injected into each BAT lobe and the incision was closed with suture. Mice were allowed to recover
427 for 3 weeks before analysis.

428 **Slit3 and Plxna1 shRNAs.** Adeno-associated viruses (AAV8) harboring three targeting shRNA
429 and one scramble control were purchased from VectorBuilder. The shRNA sequences are listed
430 in Supplementary Table 1. The three shRNAs were mixed and injected into BAT at the dose of
431 5e+11 genomic copies per lobe.

432 **AAV constructs for the overexpression of Slit3 fragments in BAT.** Mouse Slit3-FL, Slit3-N,
433 and Slit3-C sequences were cloned from a cDNA clone (Origene MR225499L4) and cloned into
434 the pAAV-hAdiponectin-W backbone[39] using NEBuilder HiFi DNA Assembly kit using the following
435 primers:

436 Slit3-FL_fwd (AACTACTCGAGgccaccATGGCCCTCGGCCGGAC),

437 Slit3-FL_rev
438 (tattcaGCGGCCGCTTAAACCTTATCGTCGTCATCCTTGTAATCgctgccGGAACACGCGCGGC
439 A), Slit3-N_fwd (AACTACTCGAGgccaccATGGCCCTCGGCCGGAC), Slit3-N_rev
440 (tattcaGCGGCCGCTTAAACCTTATCGTCGTCATCCTTGTAATCgctgccAACCATGGGTGGGG
441 G), Slit3-C_fwd (tgctgccgccCTGCTACAAACCAGCCCC), Slit3-C_rev
442 (ggttgattatcttctagagcTTACTTGTCGTCATCGTCTTTG), Signal peptide_fwd
443 (tgattccataccagagggtcGCCACCATGGCCCTCGGC), and Signal peptide_rev
444 (tttgtagcagGGCGGCAGCAGGGGGTCC).

445 pAAV-Adipoq-GFP construct[39] was used as the control. AAV8-adipoq-Slit3FL, AAV8-adipoq-
446 Slit3N, AAV8-adipoq-Slit3C, and AAV-Adipoq-GFP were packaged at VectorBuilder. 2e+10 AAV
447 particles were injected into each BAT lobe.

448 **Fluorescence-activated Cell Sorting (FACS).** Adipocytes and the Stromal Vascular Fraction
449 (SVF) were isolated from mouse BAT following the procedure described previously[5]. The
450 interscapular BAT was dissected, finely minced, and digested for 45 minutes using a cocktail
451 containing type 1 collagenase (1.5 mg ml−1; Worthington Biochemical), dispase II (2.5 U ml−1;
452 Stemcell Technologies), and fatty acid-free BSA (2%; Gemini Bio-Products) in Hanks' balanced
453 salt solution (Corning Hanks' Balanced Salt Solution, with calcium and magnesium). The resulting
454 dissociated tissue was subsequently centrifuged at 500g and 4°C for 10 minutes. Adipocytes,
455 located in the uppermost layer, were gently collected using a wide-mouthed transfer pipette and
456 filtered through a 100 μm cell strainer. Brown adipocytes were allowed to float for 5 min at room
457 temperature before they were centrifuged at 30g for 5 minutes at room temperature. This cycle
458 was repeated three times, after which the adipocytes were immediately lysed in Trizol. For the
459 SVF isolation, the pellet was resuspended in 10 ml of 10% FBS in DMEM, filtered through a 100
460 μm cell strainer into a fresh 50-ml tube, and subsequently centrifuged at 500g for 7 minutes. Red
461 blood cells were lysed in 2 ml of sterile ammonium–chloride–potassium lysis buffer (ACK Lysing
462 Buffer, Lonza) for 5 minutes on ice. The cells were then filtered once more through a 40-μm cell
463 strainer, washed with 20 ml of a solution containing 10% FBS in DMEM, and centrifuged at 500g
464 for 7 minutes. The cells were resuspended in 1 ml of Cell Staining Buffer (BioLegend) before
465 proceeding with staining.

466 Cells were stained using the fluorescently conjugated antibodies as outlined in Supplementary
467 Table 2. The cells were then incubated with the antibodies at the specified dilutions from
468 Supplementary Table 2 for a duration of 30 minutes, followed by two rounds of washing in Cell
469 Staining Buffer (BioLegend). Cells were sorted using an SH800 sorter using a 100 μm sorting
470 chip (Sony Biotechnology). Debris and doublets were excluded based on forward and side scatter
471 gating, and 7-AAD was used to exclude dead cells. Following sorting, cells were centrifuged at

472 300 g for 5 minutes and lysed in Trizol for subsequent RNA isolation and gene expression
473 analysis.

474 **RNA isolation and quantitative reverse transcription-PCR (qRT-PCR)**. RNA was isolated from
475 cells or tissues using phenol–chloroform extraction and isopropanol precipitation. qRT PCR
476 assays were conducted using a QuantStudio™ 5 Real-Time PCR instrument (Life Technologies
477 Corporation) and SYBR Green (Invitrogen). Relative mRNA expression was determined using the
478 ΔCt method and normalized to the expression of housekeeping genes Rplp0 or Tbp. Primer
479 sequences are available in Supplementary Table 3.

480 **Western blotting**. Cells or tissues were lysed in RIPA buffer supplemented with a protease
481 inhibitor cocktail (cOmplete™, Sigma-Aldrich, Dallas, TX). The primary antibodies are listed in
482 Supplementary Table 2. Primary antibodies were incubated overnight at 4 °C. HRP-coupled
483 secondary antibodies were used at 1:3000 dilution for 1 hour at room temperature. Proteins were
484 detected using the Amersham enhanced chemiluminescence (ECL) prime (GE healthcare,
485 Pittsburgh, PA) using an Odyssey M Imaging System. All the original uncropped and unprocessed
486 scans are provided in the Source Data file. For protein detection in the conditioned media, serum-
487 free and Phenol Red-free media were collected and centrifuged at 300 g to remove cell debris.
488 The supernatant was concentrated using Amicon™ Ultra-4 Centrifugal Filter Units (UFC801024,
489 MilliporeSigma™).

490 **Immunohistochemistry**. Adipose tissues were fixed in 10% formalin and embedded in paraffin.
491 5 μm sections were prepared and stained with the primary antibodies listed in Supplementary
492 Table 2. Sections were deparaffinized and rehydrated, followed by an antigen retrieval step in
493 Rodent Decloaker buffer using the Decloaking Chamber™ NxGen (BIOC Medical) in 1X rodent
494 antigen retrieval reagent (95 °C for 45 minutes). Sections were then incubated in Sudan Black
495 (0.3% in 70% ethanol) to reduce the autofluorescence signal. Blocking was performed in 5% BSA

496 in PBST (0.1% Tween-20 in PBS) for 30 minutes at room temperature, followed by incubating the
497 section in primary antibodies diluted in 1% BSA in PBST overnight at 4 °C (Supplementary Table
498 2). The biotinylated isolectin B4 was diluted in 5 ug/ml in a staining buffer containing 0.1mM
499 CaCl2, 0.1mM MgCl2, and 0.1mM MnCl2. The next day, slides were washed with PBST and were
500 incubated with appropriate fluorescently labeled secondary antibodies at a 1:200 dilution
501 (Supplementary Table 2). Slides were stained with DAPI and mounted in a mounting medium.
502 Images were collected on a Leica SP8 confocal microscope and processed with ImageJ.

503 **H&E staining**. Adipose tissues were fixed in 10% formalin and embedded in paraffin. 5 μm
504 sections were prepared and stained with hematoxylin and eosin (H&E) as previously described[40].
505 Slides were imaged using an Aperio slide scanner (Leica Biosystems).

506 **Indirect calorimetry**. Mice were individually housed in metabolic cages of a TSE Phenomaster
507 system to obtain measurements for the volume of oxygen consumption (VO2), the volume of
508 carbon dioxide production (VCO2), respiratory exchange ratio (RER), energy expenditure, food
509 intake, and locomotor activity. Mice had ad libitum access to drinking water and standard rodent
510 chow. Measurements were collected first for 48 hours at room temperature, followed by the
511 second 48 hours at 5 °C. Data were analyzed using CalR[41].

512 **Dual Energy X-ray Absorptiometry**. Lean and mass were quantified using a Dual Energy X-ray
513 Absorptiometry (DEXA) scanner (Insight, Osteosys).

514 **Tissue clearing and imaging.** Whole BAT sympathetic innervation visualization was achieved
515 using the Adipo-Clear protocol[42] with some modifications. One lobe of BAT from each animal was
516 fixed in 3% glyoxal at 4°C overnight. The fixed samples were washed in PBS three times, each
517 time for one hour. Next, the samples were subjected to a series of methanol washes: 20%, 40%,
518 60%, 80% methanol in H2O/0.1% Triton X-100/0.3 M glycine (B1N buffer, pH 7), and finally 100%

519 methanol, each for 30 minutes. Subsequently, the samples underwent a triple 30-minute
520 delipidation process with 100% dichloromethane (DCM; Sigma-Aldrich) followed by two 30-
521 minute washes in 100% methanol. After delipidation, the tissues were bleached overnight at 4°C
522 with 5% H2O2 in methanol (1 volume of 30% H2O2 to 5 volumes of methanol). The rehydration
523 process followed a reversed methanol/B1N buffer series: 80%, 60%, 40%, 20% methanol in B1N
524 buffer, each step lasting 30 minutes. All the above steps were conducted at 4°C with continuous
525 shaking. Subsequently, samples were washed in B1N buffer twice, each time for 30 minutes,
526 followed by two 1-hour wash in PBS/0.1% Triton X-100/0.05% Tween 20/2 µg/ml heparin (PTwH
527 buffer), before initiating the staining procedure. The samples were incubated with anti-tyrosine
528 hydroxylase antibody (1:200, AB1542, Millipore Sigma) in PTxwH for 4 days. After the primary
529 antibody incubation, the samples underwent a series of PTxwH washes lasting 5 min, 10 min, 15
530 min, 30 min, 1 hr, 2 hr, 4 hr, and overnight, and then were incubated in donkey anti-sheep IgG
531 Alexa Fluor 647 (1:200, A-21099, Thermo Fisher) in PTxwH for 4 days. Finally, the samples were
532 washed in PTwH for 5 min, 10 min, 15 min, 30 min, 1 hr, 2 hr, 4 hr, and overnight. Finally, the
533 samples were dehydrated using a methanol/H2O series (25%, 50%, 75%, 100%, 100%) for 30
534 minutes at each step at room temperature. Following dehydration, samples were incubated with
535 100% DCM for 30 minutes twice, followed by an overnight clearing step in dibenzyl ether (DBE;
536 Sigma-Aldrich). The samples were then stored at room temperature in the dark until imaging.
537 Representative samples were imaged by a blinded experimenter using a Zeiss Lightsheet Z.1
538 Microscope with two 1920 × 1920-pixel sCMOS cameras. Three-dimensional reconstructions
539 were generated using Imaris (Bitplane).

540 **Cloning of SNAP- and Halo-tagged Slit3 Plasmids**. pRP[Exp]-CMV>[SNAP-Slit3-HaloTag],
541 pRP[Exp]-CMV>[Slit3-FL]-HaloTag, and pRP[Exp]-CMV>[Slit3-C-HaloTag] constructs were
542 generated by VectorBuilder. The N-terminal tag was added immediately downstream of the
543 signal peptide (aa 2-33,

544 GCCCTCGGCCGGACCGGGGCCGGCGCCGCTGTGCGCGCCCGCCTGGCGCTGGGCTTGG
545 CGCTTGCGAGCATCCTGAGCGGACCCCCTGCTGCCGCC).

546 The ORF in the pRP[Exp]-CMV>[SNAP-Slit3UC-Halo] was generated by the deletion of a 27 bp
547 sequence encoding the Slit cleavage site (CCCACCCATGGTTCTGCTACAAACCAG,
548 PPPMVLLQ) from Slit3-FL cDNA.

549 **Transient transfection**. Immortalized brown preadipocytes were transfected with Slit3
550 overexpression plasmids, Bmp1 or scramble siRNA (Dharmacon GE) using Lipofectamine™
551 3000 or Lipofectamine™ RNAiMAX Transfection Reagents (Invitrogen™) following the
552 manufacturer's instructions.

553 **Bmp1 inhibitor treatment**. Cells were treated with the Bmp1 inhibitor, UK-383,367 (PZ0156-
554 5MG, Sigma Aldrich) at the final concentration of 2.5 μM.

555 **AlphaFold Multimer Analysis**. AlphaFold2 Multimer was used to predict the protein-protein
556 interactions between the extracellular domains of human PLXNA1 and the C-terminal region of
557 the Slit3 protein as described previously[43,44]. Briefly, a local graphics processing unit (GPU) cluster
558 using MMseqs (git@92deb92) was utilized for local Multiple Sequence Alignment (MSA)
559 creation[45], and ColabFold (git@7227d4c) was executed for structure prediction with 5 models per
560 prediction, including structure relaxation[46]. Predictions with an average iPTM score of >0.5 were
561 ranked, and diagnostic plots (PAE plot, pLDDT plot, and sequence coverage) were manually
562 inspected. The generated three-dimensional (3D) models of protein-protein complexes were
563 analyzed using UCSF Chimera[47] and the PyMOL Molecular Graphics System, Version 3.0
564 Schrödinger, LLC.

565 **Human data.** The human data used in this research were sourced from the Leipzig Obesity
566 Biobank (LOBB, https://www.helmholtz-munich.de/en/hi-mag/cohort/leipzig-obesity-bio-bank-

567 lobb), which comprises paired samples of abdominal subcutaneous and omental visceral adipose
568 tissue. The metabolically healthy versus unhealthy obese cohort (MHO/MUO) comprises paired
569 samples of omental visceral and abdominal subcutaneous tissues from 31 insulin-sensitive
570 patients (71% female; age: 38.8 ± 11.1 years old; BMI: 45.9 ± 6.9 kg/m²; fasting plasma glucose:
571 5.2 ± 0.2 mmol/l; fasting plasma insulin: 27.9 ± 13.5 pmol/l) and 42 insulin-resistant patients
572 (71.43% female; age: 47.2 ± 7.7 years old; BMI: 47.3 ± 8.1 kg/m²; fasting plasma glucose: 5.7 ±
573 0.3 mmol/l; fasting plasma insulin: 113.7 ± 45.7 pmol/l). The cross-sectional cohort (CSC)
574 comprises 1,479 individuals, categorized as either normal/overweight (N = 31; 52% women; age:
575 55.8 ± 13.4 years; BMI: 25.7 ± 2.7 kg/m²) or obese (N = 1,448; 71% women; age: 46.9 ± 11.7
576 years; BMI: 49.2 ± 8.3 kg/m²). Adipose tissue samples were collected during elective laparoscopic
577 abdominal surgeries, following established protocols[48,49]. Body composition and metabolic
578 parameters were assessed using standardized techniques as described previously[50,51]. The study
579 was approved by the Ethics Committee of the University of Leipzig (approval number: 159-12-
580 21052012) and adhered to the principles outlined in the Declaration of Helsinki. All participants
581 provided written informed consent before being included in the study. Exclusion criteria included
582 individuals under 18 years of age, those with chronic substance or alcohol abuse, smoking within
583 the 12 months prior to surgery, acute inflammatory conditions, concurrent use of glitazones, end-
584 stage malignancies, weight loss greater than 3% in the three months leading up to surgery,
585 uncontrolled thyroid disorders, and Cushing's disease.

586 Ribosomal RNA-depleted RNA sequencing data we generated following the SMARTseq
587 protocol[52]. The libraries were sequenced as single-end reads on a Novaseq 6000 (Illumina, San
588 Diego, CA, USA) at the Functional Genomics Center Zurich, Switzerland. The preprocessing
589 procedures were conducted as previously described[53]. In brief, adapter and quality-trimmed reads
590 were aligned to the human reference genome (assembly GRCh38.p13, GENCODE release 32),
591 and gene-level expression quantification was performed using Kallisto[54] v0.48. For samples with

592 read counts exceeding 20 million, we downsampled them to 20 million reads utilizing the R
593 package ezRun v3.14.1 (https://github.com/uzh/ezRun, accessed on April 27, 2023). The data
594 normalization was carried out using a weighted trimmed mean (TMM) of the log expression ratios,
595 with adjustments made for age, sex, and transcript integrity numbers (TINs). Analyses were
596 conducted in R v4.3.1 (www.R-project.org). Spearman coefficient was used to assess the
597 correlation between *SLIT3* expression and metabolic parameters.

598 **Data reporting.** No statistical methods were used to predetermine the sample size. Experiments
599 were not randomized. All imaging and quantifications were performed in a blinded manner.
600 Statistical analyses were performed using GraphPad Prism.

601 **Data availability**

602 The data supporting the findings of this study are available within the paper and its supplementary
603 information files. The human RNA-seq data from the LOBB have not been deposited in a public
604 repository due to restrictions imposed by patient consent but can be obtained from Matthias
605 Blüher upon request.

606

607

608 **Acknowledgment**

609 This work was supported in part by the US National Institutes of Health (grants K01DK125608,
610 R03DK135786, R01DK136724), an award from The G. Harold and Leila Y. Mathers Charitable
611 Foundation, the American Heart Association Career Development Award, and a grant from
612 Einstein-Mount Sinai Diabetes Center (to F.S.) and by National Institutes of Health grant
613 RC2DK129961 (to P.C.). The Albert Einstein Animal Physiology Core is supported by the NIH
614 grant DK20541. M.B. received funding from grants from the DFG project number 209933838 –
615 SFB 1052 (project B1) and by Deutsches Zentrum für Diabetesforschung (DZD, Grant:

82DZD00601). The Slit3 floxed strain was kindly provided by Dr. Matthew Greenblatt. We thank Adam Mar and Begona Gamallo-Lana at the NYU Langone Rodent Behavior Laboratory (RRID: SCR_017942) for providing technical assistance, Experimental Pathology Research Laboratory (RRID:SCR_017928), Preclinical Imaging Laboratory (RRID:SCR_017937), and Microscopy Laboratory (RRID: SCR_017934). The microscopy shared resource is partially supported by Cancer Center Support Grant P30CA016087. We thank Christian Wolfrum's group for contributing to the LOBB human adipose tissue RNA sequencing.

Author Contributions

T.D.S. and F.S. conceptualized the work and designed research. T.D.S., B.F., H.C., Q.T., and D.H. performed research and analyzed data. A.G. and H.A. performed the AlphaFold Multimer Analysis. C.H.J.C. and P.C. provided the adipocyte secretome data. A.H. performed RNA sequencing and preprocessing of the LOBB data. M.B. provided the data from the LOBB cohorts. G.J.S helped in designing the experiments and provided feedback. F.S. wrote the manuscript with input from all authors.

Competing interests

M.B. received honoraria as a consultant and speaker from Amgen, AstraZeneca, Bayer, Boehringer-Ingelheim, Lilly, Novo Nordisk, Novartis, and Sanofi. All other authors declare no conflict of interest.

642

643 **References**

644 1 Cannon, B. & Nedergaard, J. Brown adipose tissue: function and physiological significance.
645 *Physiol Rev* **84**, 277-359, doi:10.1152/physrev.00015.2003 (2004).
646 2 Shamsi, F., Wang, C. H. & Tseng, Y. H. The evolving view of thermogenic adipocytes -
647 ontogeny, niche and function. *Nat Rev Endocrinol* **17**, 726-744, doi:10.1038/s41574-021-
648 00562-6 (2021).
649 3 Xue, Y. *et al.* Hypoxia-independent angiogenesis in adipose tissues during cold
650 acclimation. *Cell Metab* **9**, 99-109, doi:10.1016/j.cmet.2008.11.009 (2009).
651 4 Takahashi, A., Shimazu, T. & Maruyama, Y. Importance of sympathetic nerves for the
652 stimulatory effect of cold exposure on glucose utilization in brown adipose tissue. *Jpn J*
653 *Physiol* **42**, 653-664, doi:10.2170/jjphysiol.42.653 (1992).
654 5 Shamsi, F. *et al.* Vascular smooth muscle-derived Trpv1(+) progenitors are a source of
655 cold-induced thermogenic adipocytes. *Nat Metab* **3**, 485-495, doi:10.1038/s42255-021-
656 00373-z (2021).
657 6 Shamsi, F., Zheng, R., Ho, L. L., Chen, K. & Tseng, Y. H. Comprehensive analysis of
658 intercellular communication in the thermogenic adipose niche. *Commun Biol* **6**, 761,
659 doi:10.1038/s42003-023-05140-2 (2023).
660 7 Cannavino, J. & Gupta, R. K. Mesenchymal stromal cells as conductors of adipose tissue
661 remodeling. *Genes Dev* **37**, 781-800, doi:10.1101/gad.351069.123 (2023).
662 8 Wang, Y. N. *et al.* Slit3 secreted from M2-like macrophages increases sympathetic activity
663 and thermogenesis in adipose tissue. *Nat Metab* **3**, 1536-1551, doi:10.1038/s42255-021-
664 00482-9 (2021).
665 9 Emont, M. P. *et al.* A single-cell atlas of human and mouse white adipose tissue. *Nature*
666 **603**, 926-933, doi:10.1038/s41586-022-04518-2 (2022).
667 10 Lin, Z., Chi, J. & Cohen, P. A Clearing Method for Three-Dimensional Imaging of Adipose
668 Tissue. *Methods Mol Biol* **2448**, 73-82, doi:10.1007/978-1-0716-2087-8_4 (2022).
669 11 Xu, R. *et al.* Targeting skeletal endothelium to ameliorate bone loss. *Nat Med* **24**, 823-833,
670 doi:10.1038/s41591-018-0020-z (2018).
671 12 Kang, S. H., Fukaya, M., Yang, J. K., Rothstein, J. D. & Bergles, D. E. NG2+ CNS glial
672 progenitors remain committed to the oligodendrocyte lineage in postnatal life and
673 following neurodegeneration. *Neuron* **68**, 668-681, doi:10.1016/j.neuron.2010.09.009
674 (2010).
675 13 Brose, K. *et al.* Slit proteins bind Robo receptors and have an evolutionarily conserved role
676 in repulsive axon guidance. *Cell* **96**, 795-806, doi:10.1016/s0092-8674(00)80590-5 (1999).
677 14 Choi, C. H. J. *et al.* LRG1 is an adipokine that promotes insulin sensitivity and suppresses
678 inflammation. *Elife* **11**, doi:10.7554/eLife.81559 (2022).
679 15 Kellermeyer, R. *et al.* Proteolytic cleavage of Slit by the Tolkin protease converts an axon
680 repulsion cue to an axon growth cue in vivo. *Development* **147**, doi:10.1242/dev.196055
681 (2020).
682 16 Talantikite, M. *et al.* Inhibitors of BMP-1/tolloid-like proteinases: efficacy, selectivity and
683 cellular toxicity. *FEBS Open Bio* **8**, 2011-2021, doi:10.1002/2211-5463.12540 (2018).

684 17 Delloye-Bourgeois, C. *et al.* PlexinA1 is a new Slit receptor and mediates axon guidance
685 function of Slit C-terminal fragments. *Nat Neurosci* **18**, 36-45, doi:10.1038/nn.3893
686 (2015).
687 18 Nguyen Ba-Charvet, K. T. *et al.* Diversity and specificity of actions of Slit2 proteolytic
688 fragments in axon guidance. *J Neurosci* **21**, 4281-4289 (2001).
689 19 Watanabe, T., Watanabe-Kominato, K., Takahashi, Y., Kojima, M. & Watanabe, R. Adipose
690 Tissue-Derived Omentin-1 Function and Regulation. *Compr Physiol* **7**, 765-781,
691 doi:10.1002/cphy.c160043 (2017).
692 20 Yang, R. Z. *et al.* Identification of omentin as a novel depot-specific adipokine in human
693 adipose tissue: possible role in modulating insulin action. *Am J Physiol Endocrinol Metab*
694 **290**, E1253-1261, doi:10.1152/ajpendo.00572.2004 (2006).
695 21 Amano, S. *et al.* Bone morphogenetic protein 1 is an extracellular processing enzyme of
696 the laminin 5 gamma 2 chain. *J Biol Chem* **275**, 22728-22735,
697 doi:10.1074/jbc.M002345200 (2000).
698 22 Kessler, E., Takahara, K., Biniaminov, L., Brusel, M. & Greenspan, D. S. Bone
699 morphogenetic protein-1: the type I procollagen C-proteinase. *Science* **271**, 360-362,
700 doi:10.1126/science.271.5247.360 (1996).
701 23 Hopkins, D. R., Keles, S. & Greenspan, D. S. The bone morphogenetic protein 1/Tolloid-
702 like metalloproteinases. *Matrix Biol* **26**, 508-523, doi:10.1016/j.matbio.2007.05.004
703 (2007).
704 24 Muir, A. M. *et al.* Induced ablation of Bmp1 and Tll1 produces osteogenesis imperfecta in
705 mice. *Hum Mol Genet* **23**, 3085-3101, doi:10.1093/hmg/ddu013 (2014).
706 25 Zhou, Y., Gunput, R.-A. F. & Pasterkamp, R. J. Semaphorin signaling: progress made and
707 promises ahead. *Trends in Biochemical Sciences* **33**, 161-170,
708 doi:https://doi.org/10.1016/j.tibs.2008.01.006 (2008).
709 26 Alto, L. T. & Terman, J. R. Semaphorins and their Signaling Mechanisms. *Methods Mol Biol*
710 **1493**, 1-25, doi:10.1007/978-1-4939-6448-2_1 (2017).
711 27 Guilherme, A., Henriques, F., Bedard, A. H. & Czech, M. P. Molecular pathways linking
712 adipose innervation to insulin action in obesity and diabetes mellitus. *Nat Rev Endocrinol*
713 **15**, 207-225, doi:10.1038/s41574-019-0165-y (2019).
714 28 Jiang, H., Ding, X., Cao, Y., Wang, H. & Zeng, W. Dense Intra-adipose Sympathetic
715 Arborizations Are Essential for Cold-Induced Beiging of Mouse White Adipose Tissue. *Cell*
716 *Metab* **26**, 686-692 e683, doi:10.1016/j.cmet.2017.08.016 (2017).
717 29 Murano, I., Barbatelli, G., Giordano, A. & Cinti, S. Noradrenergic parenchymal nerve fiber
718 branching after cold acclimatisation correlates with brown adipocyte density in mouse
719 adipose organ. *J Anat* **214**, 171-178, doi:10.1111/j.1469-7580.2008.01001.x (2009).
720 30 Bougneres, P. *et al.* In vivo resistance of lipolysis to epinephrine. A new feature of
721 childhood onset obesity. *J Clin Invest* **99**, 2568-2573, doi:10.1172/JCI119444 (1997).
722 31 Heinonen, S. *et al.* Impaired Mitochondrial Biogenesis in Adipose Tissue in Acquired
723 Obesity. *Diabetes* **64**, 3135-3145, doi:10.2337/db14-1937 (2015).
724 32 Guo, T. *et al.* Adipocyte ALK7 links nutrient overload to catecholamine resistance in
725 obesity. *Elife* **3**, e03245, doi:10.7554/eLife.03245 (2014).

33 Pirzgalska, R. M. *et al.* Sympathetic neuron-associated macrophages contribute to obesity by importing and metabolizing norepinephrine. *Nat Med* **23**, 1309-1318, doi:10.1038/nm.4422 (2017).
34 Saxton, S. N., Withers, S. B. & Heagerty, A. M. Emerging Roles of Sympathetic Nerves and Inflammation in Perivascular Adipose Tissue. *Cardiovasc Drugs Ther* **33**, 245-259, doi:10.1007/s10557-019-06862-4 (2019).
35 Daily, J. W., Liu, M. & Park, S. High genetic risk scores of SLIT3, PLEKHA5 and PPP2R2C variants increased insulin resistance and interacted with coffee and caffeine consumption in middle-aged adults. *Nutr Metab Cardiovasc Dis* **29**, 79-89, doi:10.1016/j.numecd.2018.09.009 (2019).
36 Liu, Y. J. *et al.* Genome-wide association scans identified CTNNBL1 as a novel gene for obesity. *Hum Mol Genet* **17**, 1803-1813, doi:10.1093/hmg/ddn072 (2008).
37 Baca, P. *et al.* DNA methylation and gene expression analysis in adipose tissue to identify new loci associated with T2D development in obesity. *Nutr Diabetes* **12**, 50, doi:10.1038/s41387-022-00228-w (2022).
38 van der Klaauw, A. A. *et al.* Human Semaphorin 3 Variants Link Melanocortin Circuit Development and Energy Balance. *Cell* **176**, 729-742 e718, doi:10.1016/j.cell.2018.12.009 (2019).
39 Shamsi, F. *et al.* FGF6 and FGF9 regulate UCP1 expression independent of brown adipogenesis. *Nat Commun* **11**, 1421, doi:10.1038/s41467-020-15055-9 (2020).
40 Berry, R. *et al.* Imaging of adipose tissue. *Methods Enzymol* **537**, 47-73, doi:10.1016/b978-0-12-411619-1.00004-5 (2014).
41 Mina, A. I. *et al.* CalR: A Web-Based Analysis Tool for Indirect Calorimetry Experiments. *Cell Metab* **28**, 656-666.e651, doi:10.1016/j.cmet.2018.06.019 (2018).
42 Chi, J., Crane, A., Wu, Z. & Cohen, P. Adipo-Clear: A Tissue Clearing Method for Three-Dimensional Imaging of Adipose Tissue. *J Vis Exp*, doi:10.3791/58271 (2018).
43 Jumper, J. *et al.* Highly accurate protein structure prediction with AlphaFold. *Nature* **596**, 583-589, doi:10.1038/s41586-021-03819-2 (2021).
44 Evans, R. *et al.* Protein complex prediction with AlphaFold-Multimer. *bioRxiv*, 2021.2010.2004.463034, doi:10.1101/2021.10.04.463034 (2022).
45 Steinegger, M. & Soding, J. MMseqs2 enables sensitive protein sequence searching for the analysis of massive data sets. *Nat Biotechnol* **35**, 1026-1028, doi:10.1038/nbt.3988 (2017).
46 Mirdita, M. *et al.* ColabFold: making protein folding accessible to all. *Nat Methods* **19**, 679-682, doi:10.1038/s41592-022-01488-1 (2022).
47 Pettersen, E. F. *et al.* UCSF Chimera--a visualization system for exploratory research and analysis. *J Comput Chem* **25**, 1605-1612, doi:10.1002/jcc.20084 (2004).
48 Langhardt, J. *et al.* Effects of Weight Loss on Glutathione Peroxidase 3 Serum Concentrations and Adipose Tissue Expression in Human Obesity. *Obes Facts* **11**, 475-490, doi:10.1159/000494295 (2018).
49 Mardinoglu, A. *et al.* Extensive weight loss reveals distinct gene expression changes in human subcutaneous and visceral adipose tissue. *Scientific Reports* **5**, 14841, doi:10.1038/srep14841 (2015).

50 Blüher, M. Metabolically Healthy Obesity. *Endocr Rev* **41**, doi:10.1210/endrev/bnaa004 (2020).
51 Klöting, N. *et al.* Insulin-sensitive obesity. *Am J Physiol Endocrinol Metab* **299**, E506-515, doi:10.1152/ajpendo.00586.2009 (2010).
52 Picelli, S. *et al.* Full-length RNA-seq from single cells using Smart-seq2. *Nat Protoc* **9**, 171-181, doi:10.1038/nprot.2014.006 (2014).
53 Hagemann, T. *et al.* Laminin α4 Expression in Human Adipose Tissue Depots and Its Association with Obesity and Obesity Related Traits. *Biomedicines* **11**, doi:10.3390/biomedicines11102806 (2023).
54 Bray, N. L., Pimentel, H., Melsted, P. & Pachter, L. Near-optimal probabilistic RNA-seq quantification. *Nat Biotechnol* **34**, 525-527, doi:10.1038/nbt.3519 (2016).

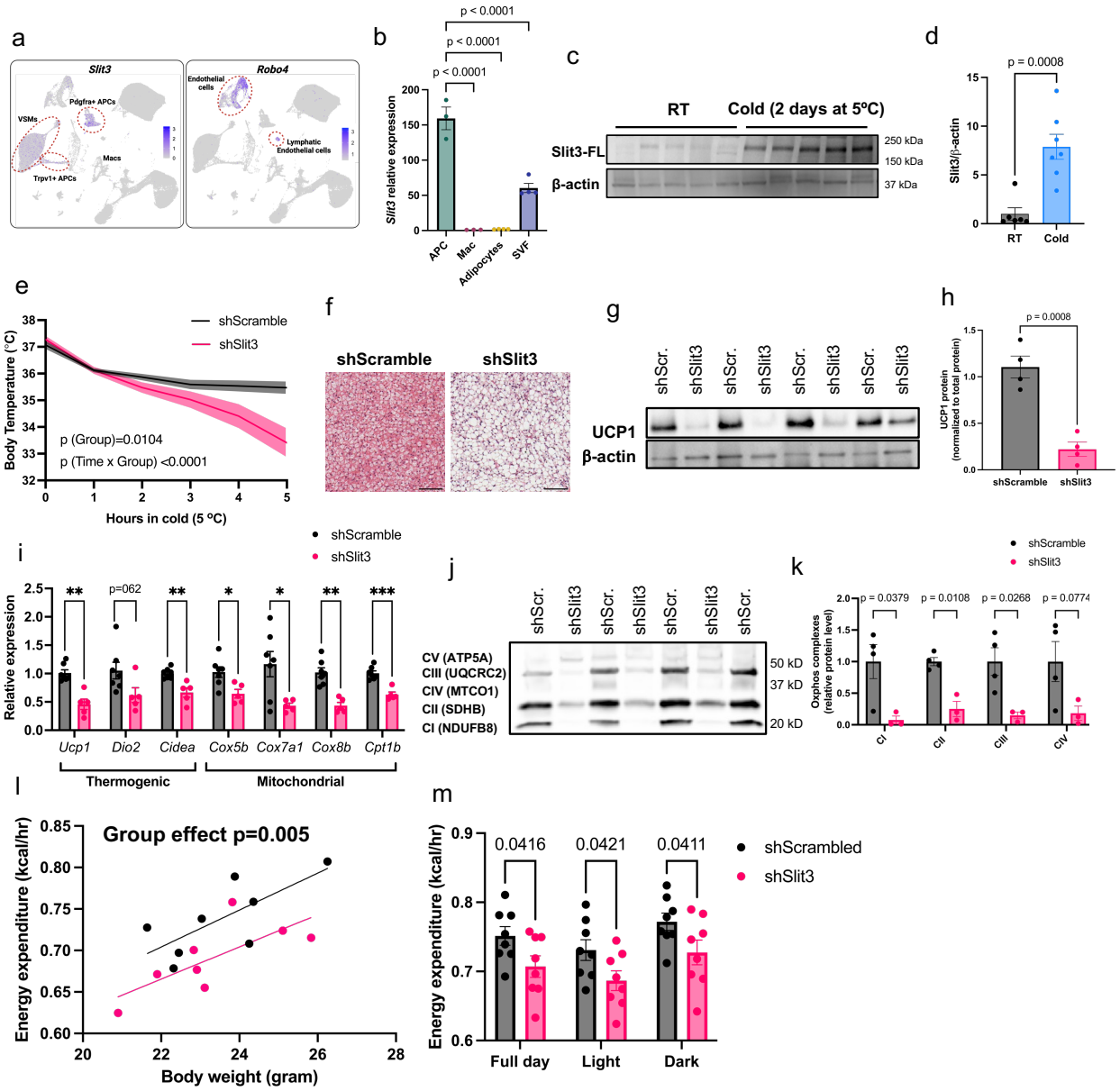

Figure 1. Axon Guidance Molecule Slit3 is essential for BAT thermogenesis.

(a) Slit3 and Robo4 expression in scRNA-seq data from mouse BAT.

(b) Slit3 expression in isolated adipocyte progenitors, macrophages, adipocytes, and the total stromal vascular fraction from mouse BAT.

(c-d) Slit3 protein levels in BAT of mice housed at room temperature (RT) or cold (5°C for 2 days).

(e) Cold tolerance test in AAV-shSlit3 or AAV-shScramble-injected mice.

(f) Representative Hematoxylin and Eosin (H&E) staining of BAT. Scale bar = 100 μm.

(g-h) UCP1 protein levels in BAT of mice after 7 days at cold (5°C).

791 (i) Expression of thermogenic and mitochondrial genes in BAT of mice after 7 days at cold
792 (5°C).
793 (j-k) OxPhos complex protein levels in BAT of mice receiving AAV-shSlit3 or scramble shRNA
794 and housed at cold (5°C) for 7 days.
795 (l) Regression plots of energy expenditure versus total body mass in AAV-shSlit3 or AAV-
796 shScramble-injected mice housed at 5°C.
797 (m) Average daily energy expenditure in AAV-shSlit3 or AAV-shScramble-injected mice housed
798 at 5°C.
799 N = 4–7 per group (b, c-d, g-k), N = 8 per group (l, m). Data are presented as means ± SEM and
800 analyzed by one-way ANOVA with Dunnett's multiple comparison test (b), repeated measures
801 ANOVA (e), unpaired two-sided Student's t-tests (h, i, k), ANCOVA (l), and two-way ANOVA
802 (m).

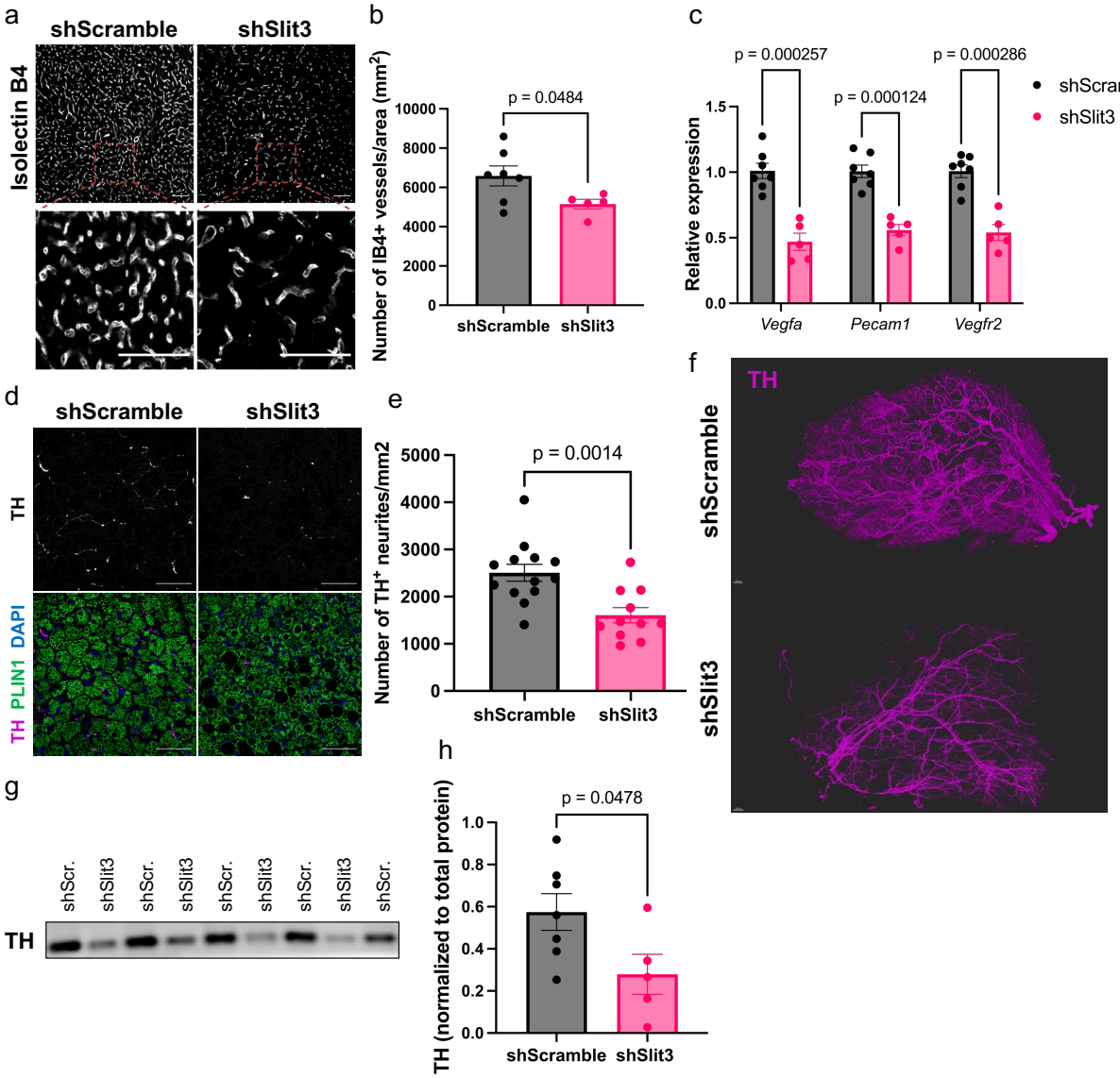

Figure 2. Loss of Slit3 impairs cold-induced angiogenesis and sympathetic innervation in BAT.

(a) Representative images of Isolectin B4 (IB4) staining in BAT of mice receiving AAV-shSlit3 or scramble shRNA after 7 days at cold (5°C). Scale bar = 50 μm.

(b) Quantification of the number of capillaries per area in BAT of mice receiving AAV-shSlit3 or scramble shRNA after 7 days at cold (5°C).

(c) Expression of endothelial cell markers in BAT of mice receiving AAV-shSlit3 or scramble shRNA after 7 days at cold (5°C).

(d) Representative images of TH and Plin1 staining in BAT of mice receiving AAV-shSlit3 or scramble shRNA after 7 days at cold (5°C). Scale bar = 50 μm.

814 (e) Quantification of TH^+ neurites per area in BAT of mice receiving AAV-shSlit3 or scramble
815 shRNA after 7 days at cold (5°C).
816 (f) 3-D reconstruction of TH staining in BAT of mice receiving AAV-shSlit3 or scramble shRNA
817 after 7 days at cold (5°C).
818 (g–h) TH protein levels in BAT of mice receiving AAV-shSlit3 or scramble shRNA after 7 days at
819 cold (5°C).
820 N = 5–7 per group. Data are presented as means ± SEM and analyzed by unpaired two-sided
821 Student's t-tests.

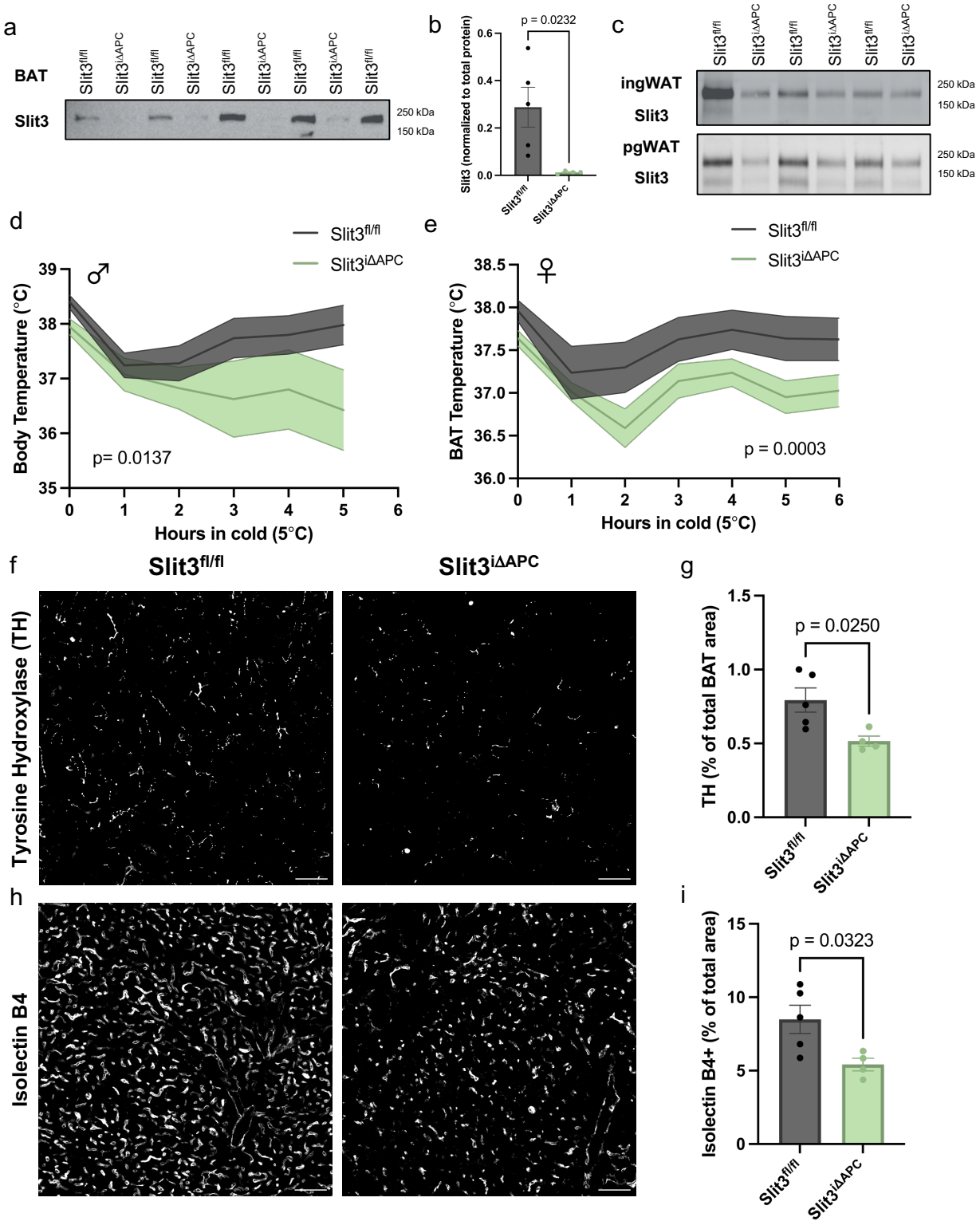
a
BAT
Slit3
Slit3fl/fl
Slit3iΔAPC
250 kDa
150 kDa
b
p = 0.0232
Slit3 (normalized to total protein)
c
ingWAT
pgWAT
d
Slit3fl/fl
Slit3iΔAPC
Body Temperature (°C)
p= 0.0137
Hours in cold (5°C)
e
BAT Temperature (°C)
p = 0.0003
f
Tyrosine Hydroxylase (TH)
g
TH (% of total BAT area)
p = 0.0250
h
Isolectin B4
i
Isolectin B4+ (% of total area)
p = 0.0323

825 **Figure 3. Adipocyte-specific Slit3 deletion impairs cold induced thermogenesis.**
826 (a-c) SLIT3 protein levels in BAT, ingWAT (c, top) and pgWAT (c bottom) depots of $Slit3^{fl/fl}$ and
827 $Slit3^{i\Delta APC}$ mice.
828 (d-e) BAT temperature during the cold tolerance test in (g) male and (h) female $Slit3^{fl/fl}$ and
829 $Slit3^{i\Delta APC}$ mice.
830 (f) Representative images of TH staining in BAT, (g) quantification of TH^{+} neurites per BAT area,
831 (h) representative images of Isolectin B4 (IB4) staining, and (i) quantification of $IB4^{+}$ capillaries
832 per BAT area in BAT of $Slit3^{fl/fl}$ and $Slit3^{i\Delta APC}$ mice after 7 days at cold (5°C). Scale bar = 50 μm.
833 N = 4–5 per group (a–c), N = 7–9 per group (d). Data are presented as means ± SEM and
834 analyzed by repeated measures ANOVA (d-e) and unpaired two-sided Student's t-tests (b, g, i).
835
836
837
838
839
840

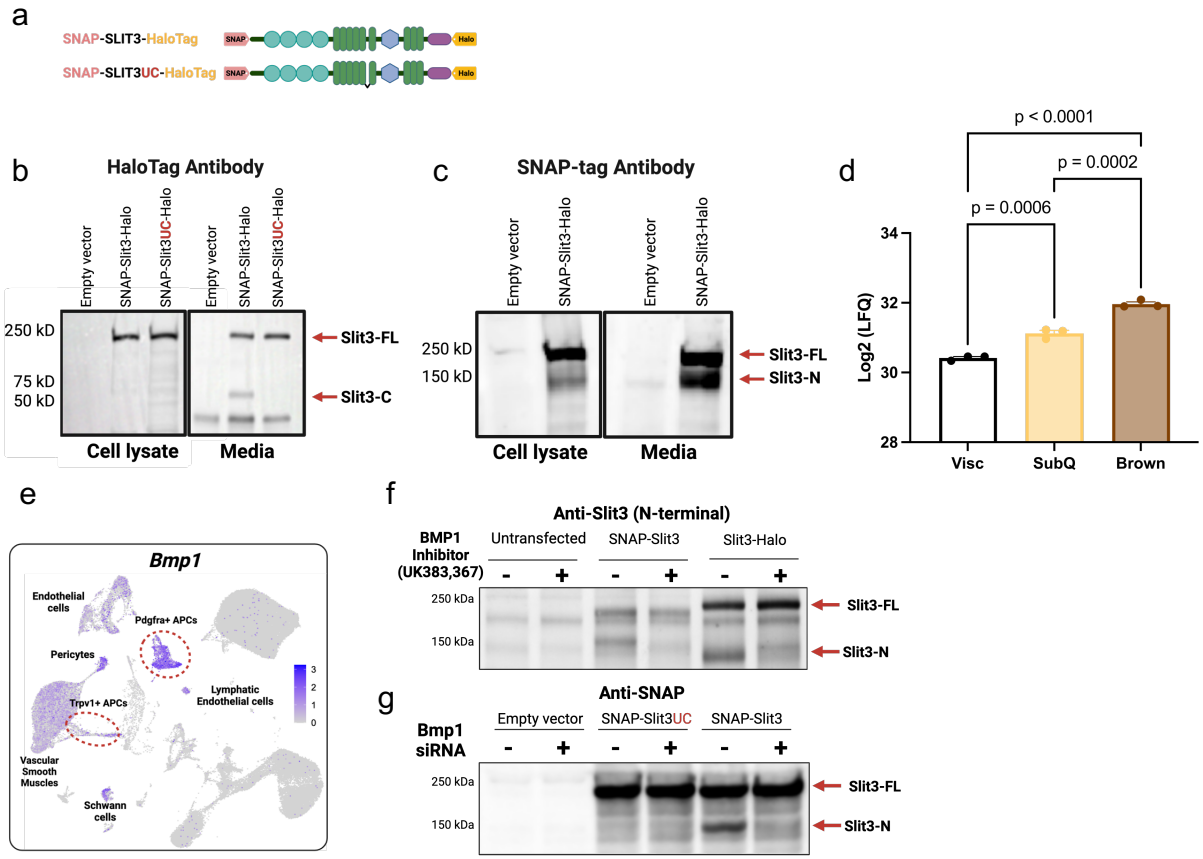

Figure 4. BMP1-mediated proteolytic cleavage of SLIT3 generates two secreted ligands.

(a) Schematic of the tagged Slit3 transgenes.

(b–c) Western blots using HaloTag (b) and SNAP-tag (c) antibodies to visualize SLIT3 fragments in cell lysates and conditioned media from adipocyte progenitors expressing the indicated plasmids.

(d) Quantification of total SLIT3 peptide area in conditioned media from in vitro differentiated primary visceral (Visc), subcutaneous (SubQ), and brown adipocytes by mass spectrometry.

(e) Expression of Bmp1 in adipocyte progenitors from scRNA-seq data of mouse BAT.

(f) Western blot for SLIT3 in adipocyte progenitors transfected with the indicated constructs and treated with Bmp1 inhibitor UK383,367 or vehicle.

(j) Western blot using SNAP-tag antibody in adipocyte progenitors transfected with siBMP1 or scrambled siRNA and overexpressing the indicated constructs.

N = 3 per group. Data are presented as mean ± SEM and analyzed by one-way ANOVA with Tukey's multiple comparisons test (d).

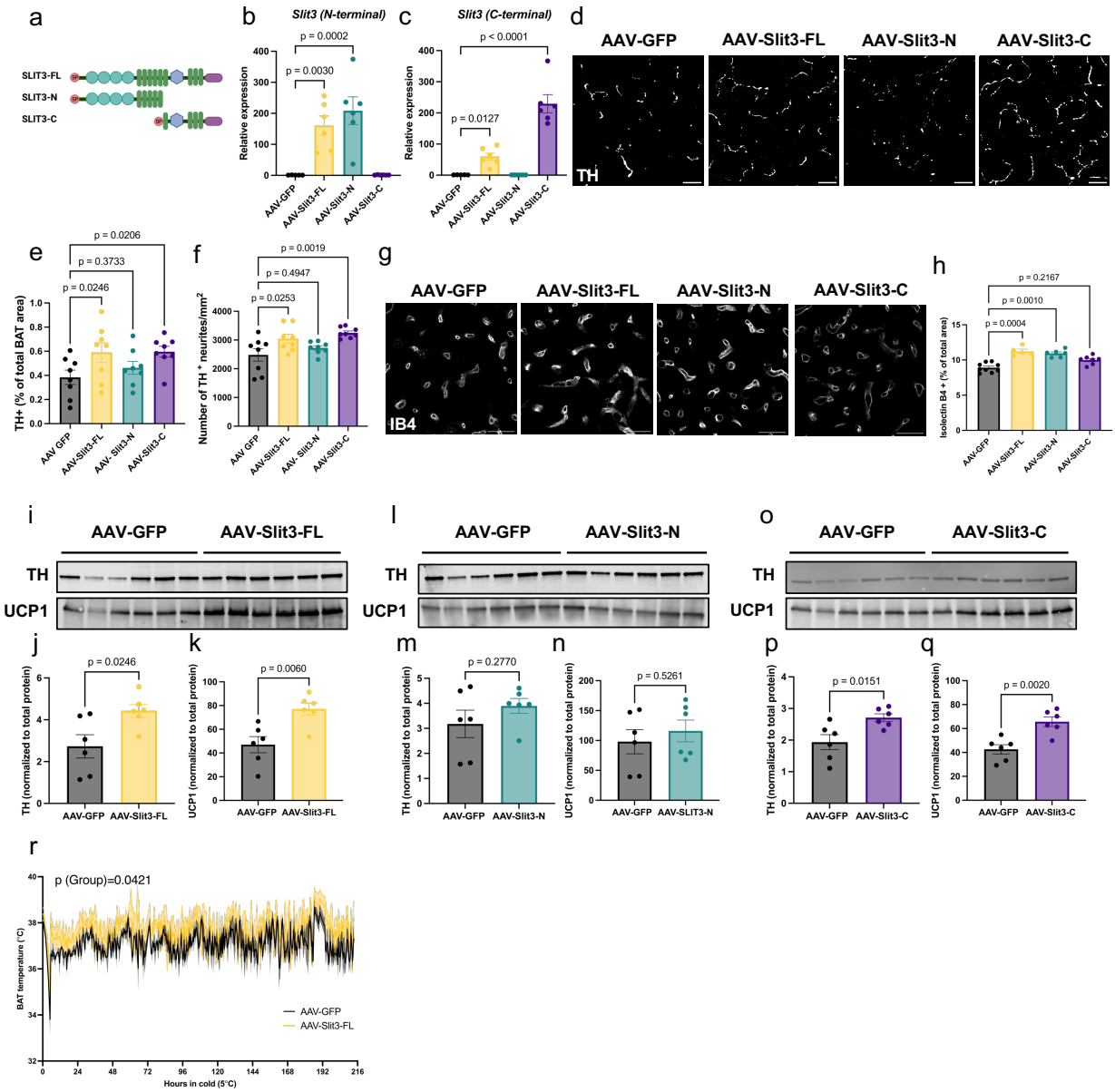

Figure 5. Slit3 fragments promote angiogenesis and sympathetic innervation in BAT.

(a) Schematic representation of Slit3-FL, Slit3-N, and Slit3-C constructs.

(b–c) Expression of Slit3 fragments in BAT measured by qPCR using primers targeting the (b) N-terminal or (c) C-terminal regions of the Slit3 transcript.

(d) Representative images of TH staining in BAT from mice expressing AAV-GFP, AAV-Slit3-FL, AAV-Slit3-N, or AAV-Slit3-C after 7 days of cold exposure (5 °C). Scale bar = 25 µm.

(e–f) Quantification of TH^+ (e) area and (f) neurite density.

(g) Representative images of Isolectin B4 staining in BAT from mice expressing AAV-GFP, AAV-Slit3-FL, AAV-Slit3-N, or AAV-Slit3-C after 7 days of cold exposure (5 °C). Scale bar = 50 μm.

(h) Quantification of Isolectin $B4^+$ capillary area in BAT.

(i–q) Western blots and quantification of TH and UCP1 in BAT from mice expressing AAV-GFP, AAV-Slit3-FL (i–k), AAV-Slit3-N (l–n), or AAV-Slit3-C (o–q) after 7 days of cold exposure (5 °C).

(r) BAT temperature during cold exposure in mice expressing AAV-GFP or AAV-Slit3-FL.

N = 6–8 per group. Data are presented as mean ± SEM and analyzed by one-way ANOVA with Dunnett's multiple comparisons test (b–c, e–f, h), unpaired two-sided Student's t-test (j–k, m–n, p–q), and a mixed-effects model with Geisser-Greenhouse correction (r).

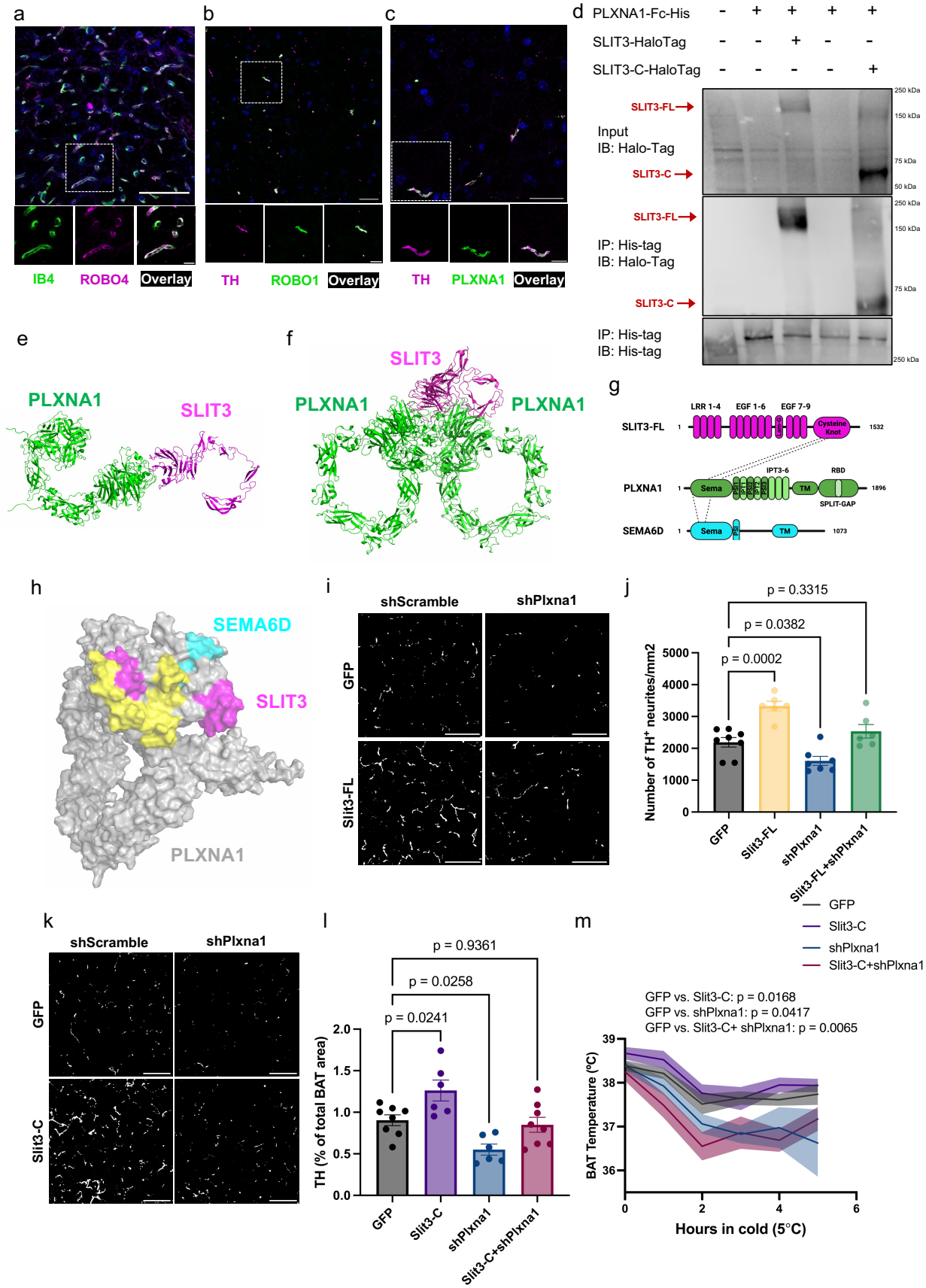
a
IB4
ROBO4
Overlay
b
TH
ROBO1
Overlay
c
TH
PLXNA1
Overlay
d
PLXNA1-Fc-His
SLIT3-HaloTag
SLIT3-C-HaloTag
SLIT3-FL
Input
IB: Halo-Tag
SLIT3-C
IP: His-tag
IB: Halo-Tag
IP: His-tag
IB: His-tag
250 kDa
150 kDa
75 kDa
50 kDa
e
PLXNA1
SLIT3
f
SLIT3
PLXNA1
PLXNA1
g
SLIT3-FL
LRR 1-4
EGF 1-6
EGF 7-9
Cysteine Knot
1532
PLXNA1
Sema
IPT3-6
TM
RBD
SPLIT-GAP
1896
SEMA6D
Sema
TM
1073
h
SEMA6D
SLIT3
PLXNA1
i
shScramble
shPlxna1
GFP
Slit3-FL
j
p = 0.3315
p = 0.0382
p = 0.0002
Number of TH+ neurites/mm2
5000
4000
3000
2000
1000
0
GFP
Slit3-FL
shPlxna1
Slit3-FL+shPlxna1
k
shScramble
shPlxna1
GFP
Slit3-C
l
p = 0.9361
p = 0.0258
p = 0.0241
TH (% of total BAT area)
2.0
1.5
1.0
0.5
0.0
GFP
Slit3-C
shPlxna1
Slit3-C+shPlxna1
m
GFP
Slit3-C
shPlxna1
Slit3-C+shPlxna1
GFP vs. Slit3-C: p = 0.0168
GFP vs. shPlxna1: p = 0.0417
GFP vs. Slit3-C+ shPlxna1: p = 0.0065
BAT Temperature (°C)
39
38
37
36
0
2
4
6
Hours in cold (5°C)

875 **Figure 6. Plxna1 is the Slit3 receptor that mediates sympathetic innervation in BAT**.

876 (a–c) Immunofluorescence co-staining in BAT: (a) ROBO4 with Isolectin B4 (vascular marker),
877 (b) ROBO1 with TH (sympathetic nerves), and (c) PLXNA1 with TH. Scale bars = 50 μm (a),
878 25 μm (b–c).

879 (d) Co-immunoprecipitation of His-tagged PLXNA1 with Halo-tagged SLIT3-FL or SLIT3-C in
880 HEK293T cells.

881 (e-f) Ribbon representations of the top-ranked monomeric PLXNA1-SLIT3 (e) and dimeric
882 PLXNA1 and monomeric SLIT3 (f) interaction models.

883 (g) Domain organization of full-length human SLIT3 (magenta), PLXNA1 (green), and
884 Semaphorin-6D (cyan). The dashed lines between SLIT3 and PLXNA1 and Semaphorin-6D
885 (SEMA6D) and PLXNA1 indicate the binding regions between these proteins. Protein sequences
886 used in this study are as follows: human PLXNA1 residues 27-1244 (UniProt ID: Q9UIW2), human
887 Slit3 residues 1120-1523 (UniProt ID: O75094), human Semaphorin-6D residues 1-1073 (UniProt
888 ID: Q8NFY4). Human SLIT3 protein comprised of an LRR: leucin-rich repeat region, an EGF-like
889 epidermal growth factor-like domain, a Lam-G like: Agrin, Laminin, Perlecan and SLIT (ALPS) or
890 laminin G-like module, and a C-terminal cysteine knot. SEMA6D consists of Sema and PSI
891 domains in the extracellular region. PLXNA1 contains a Sema domain, three PSI domains, and
892 six IPT (immunoglobulin-like, plexins, and transcription factors) domains in the extracellular
893 domain, while a GAP (GTPase-activating protein) domain split by RBD (Rho-binding domain),
894 termed as Split-GAP, is present in the cytoplasmic domain.

895 (h) Human SLIT3 and SEMA6D interaction interfaces mapped on the molecular surfaces of
896 PLXNA1 extracellular domains (residues 27-1244) AlphaFold2 model. The SLIT3 and SEMA6D
897 binding interfaces are shown in magenta and cyan, respectively. The common binding footprint
898 is colored in yellow.

899 (i) Representative TH-stained images and (j) quantification of TH^+ area in BAT of mice expressing
900 Slit3-FL with or without shPlxna1 after 7 days of cold exposure (5 °C). Scale bar = 50 μm.

901 (k) Representative TH-stained images and (l) quantification of TH^+ area in BAT of mice expressing
902 Slit3-C with or without shPlxna1 after 3 days of cold exposure (5 °C). Scale bar = 50 μm.

903 (m) BAT temperature during the cold tolerance test in mice expressing Slit3-C with or without
904 shPlxna1.

905 N = 6–8 mice per group. Data are presented as mean ± SEM. Statistical analysis was performed
906 using one-way ANOVA with Dunnett's multiple comparisons test (f, h) and repeated measures
907 ANOVA with Dunnett's test (i).
908
909
910
911

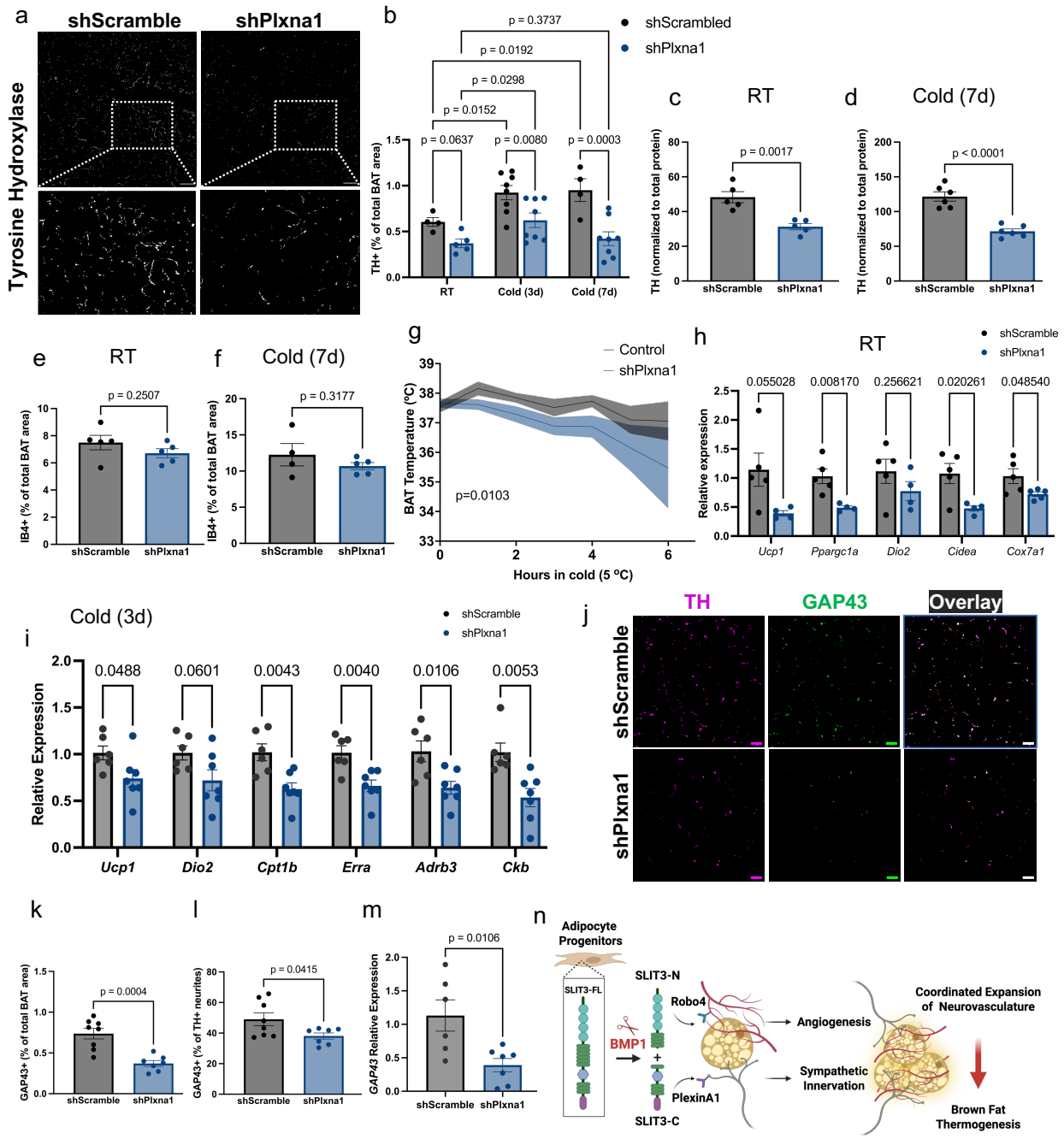

Figure 7. Plxna1 is essential for sympathetic innervation and cold-induced neurite expansion in BAT.

All mice were injected with AAV-shPlxna1 or scramble shRNA in BAT.

(a) Representative images of tyrosine hydroxylase (TH) staining in BAT. Scale bar = 50 μm.

(b) Quantification of TH+ area in BAT from mice housed at room temperature (RT) or exposed to cold (5°C) for 3 or 7 days.

919 (c–d) Total TH protein levels in BAT from mice housed at (c) RT or (d) cold (5°C) for 7 days.

920 (e–f) Capillary density in BAT from mice housed at (e) RT or (f) cold (5°C) for 7 days.

921 (g) BAT temperature during the cold tolerance test.

922 (h–i) Expression of thermogenic and mitochondrial genes in BAT from mice housed at (h) RT or
923 (i) cold (5°C) for 3 days.

924 (j) Representative images of tyrosine hydroxylase (TH) and GAP43 staining in BAT from mice
925 housed at cold (5°C) for 3 days. Scale bar = 20 μm.

926 (k-l) Quantification of $GAP43^+$ area (k) and percentage of TH^+ neurites co-expressing GAP43 (l)
927 in BAT from mice housed at 5°C for 3 days.

928 (k) GAP43 expression in BAT from mice housed at cold (5°C) for 3 days.

929 (n) Proposed model of BAT neurovascular remodeling regulated by Slit3 fragments.

930 N = 4–8 mice per group. Data are presented as mean ± SEM. Statistical analysis was performed
931 using two-way ANOVA with multiple comparisons correction (Benjamini, Krieger, and Yekutieli)
932 for (b); unpaired, two-sided Student's t-test for (c–f, h–i, k-m); and paired, two-sided Student's t-
933 test for (g).

934

935

936

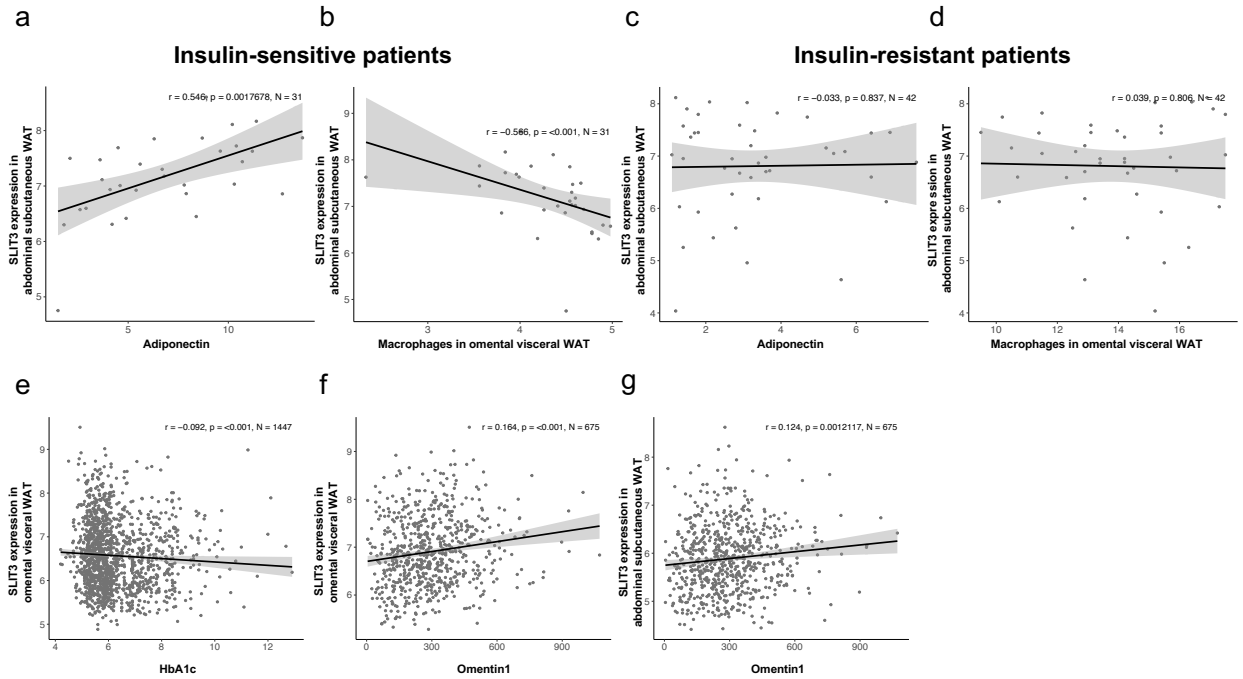

Figure 8. Slit3 expression is associated with adipose tissue health and inflammation in humans.

Spearman correlations between SLIT3 expression in adipose tissue and metabolic or inflammatory markers in human cohorts.

(a–b) In insulin-sensitive individuals, SLIT3 expression in abdominal subcutaneous WAT correlates with (a) adiponectin and (b) macrophage content in omental visceral WAT.

(c–d) In insulin-resistant individuals, SLIT3 expression in abdominal subcutaneous WAT correlates with (c) adiponectin and (d) macrophages in omental visceral WAT.

(e–f) In omental visceral WAT, SLIT3 expression correlates with (e) HbA1c and (f) Omentin1 levels.

(g) SLIT3 expression in abdominal subcutaneous WAT correlates with Omentin1 levels.

Spearman correlation coefficient (r), p-value (p), and sample size (N) are indicated on each plot. Gene expression values represent weighted trimmed mean (TMM) of log expression ratios.

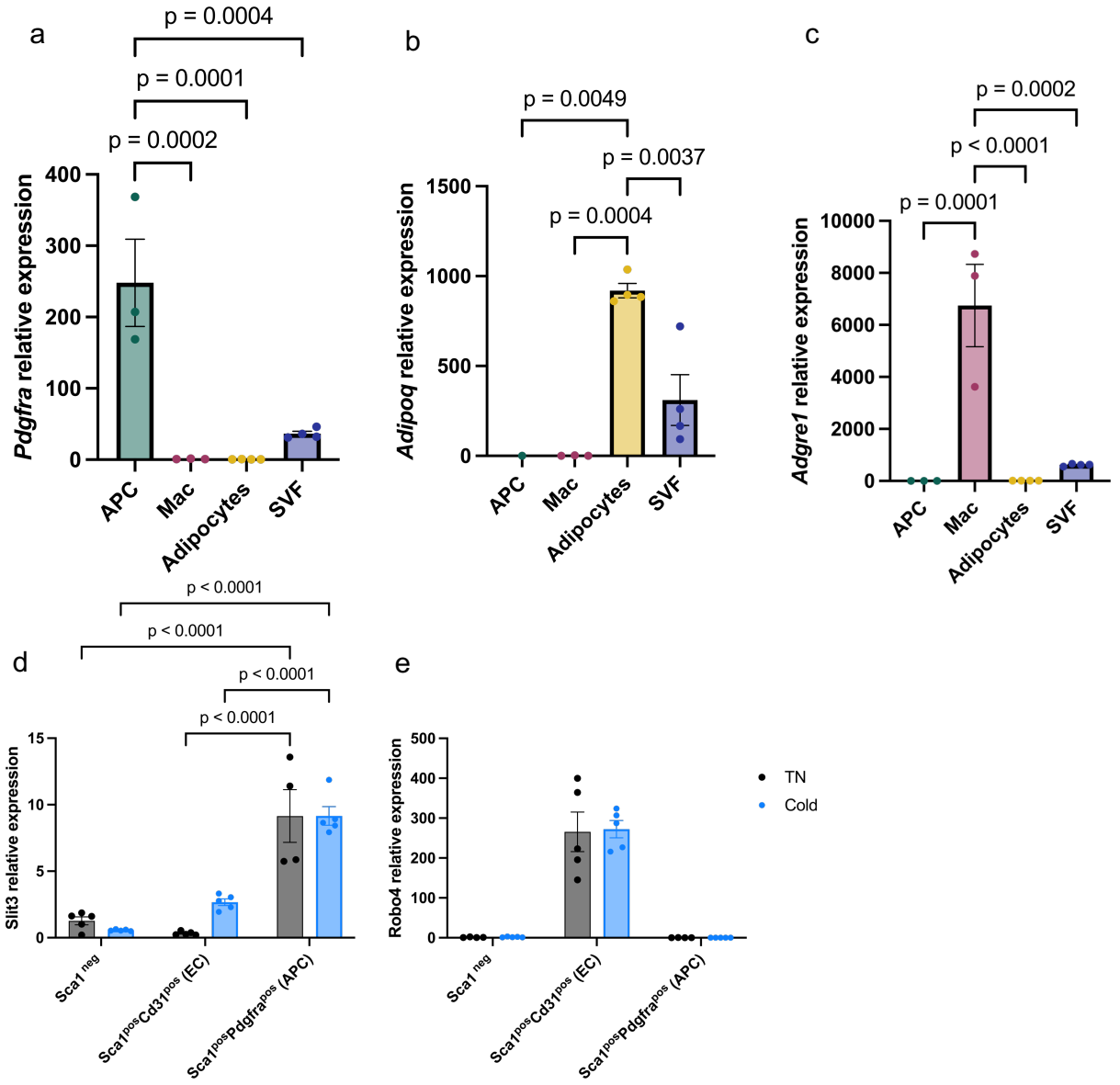

Supplementary Figure 1. Related to Figure 1.

(a–c) Expression of *Pdgfra*, *Adipoq*, and *Adgre1* in isolated adipocyte progenitors, macrophages, adipocytes, and total stromal vascular fraction (SVF) from mouse BAT.

(d–e) Expression of *Slit3* and *Robo4* in Sca1^{-}, Sca1^{+}Cd31^{+}, and Sca1^{+}Pdgfra^{+} cells isolated from BAT of mice housed at thermoneutrality (30 °C) or cold (5 °C) for 7 days.

N = 3–5 per group. Data are presented as mean ± SEM and analyzed by one-way ANOVA with Dunnett's multiple comparisons test (a–c) and two-way ANOVA with Tukey's multiple comparisons test (d–e).

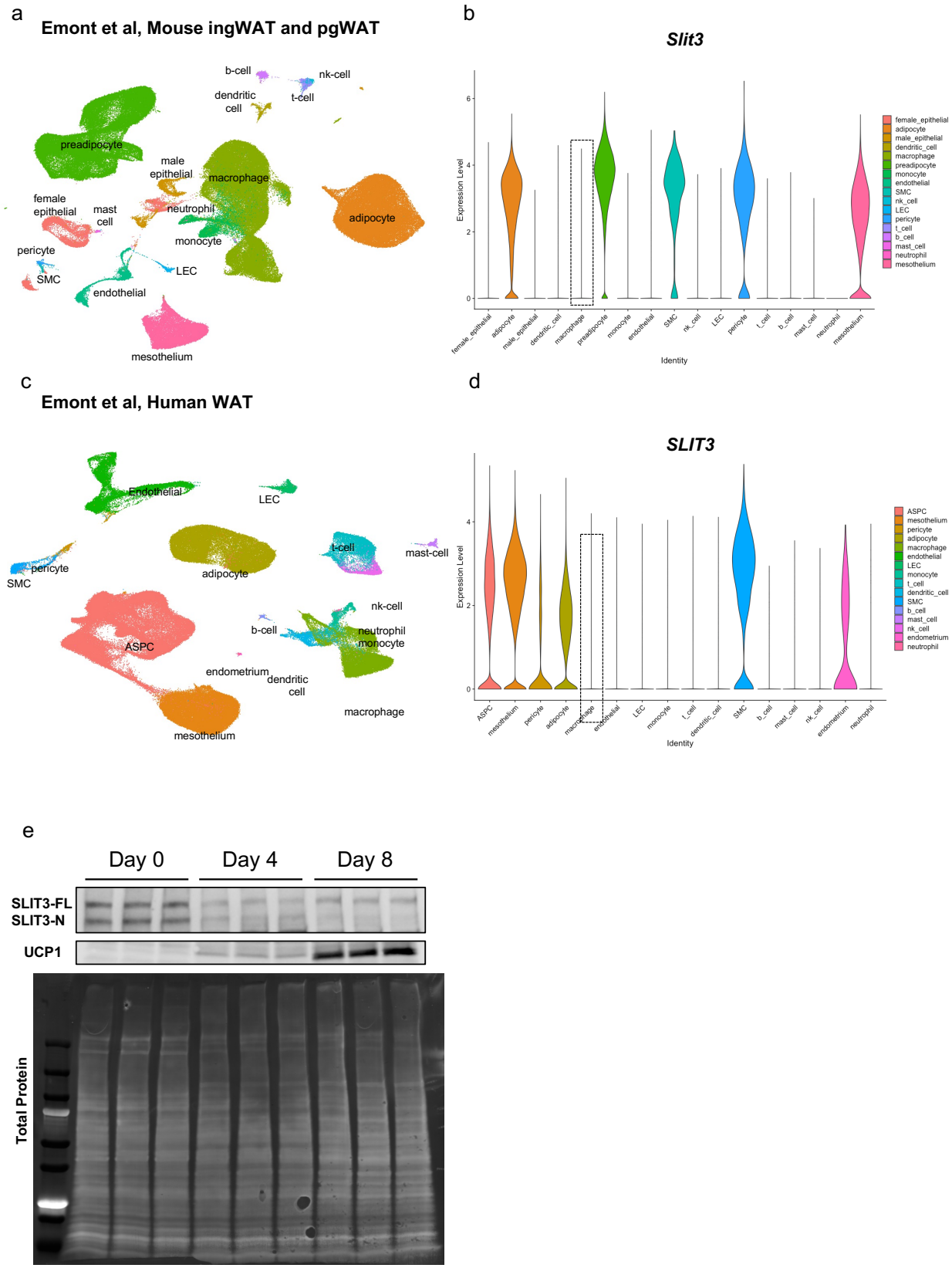
a
Emont et al, Mouse ingWAT and pgWAT
b-cell
nk-cell
dendritic cell
t-cell
preadipocyte
male epithelial
macrophage
female epithelial
mast cell
neutrophil
adipocyte
monocyte
pericyte
SMC
LEC
endothelial
mesothelium
b
Slit3
Expression Level
Identity
female_epithelial
adipocyte
male_epithelial
dendritic_cell
macrophage
preadipocyte
monocyte
endothelial
SMC
nk_cell
LEC
pericyte
t_cell
b_cell
mast_cell
neutrophil
mesothelium
c
Emont et al, Human WAT
Endothelial
LEC
t-cell
mast-cell
pericyte
SMC
adipocyte
nk-cell
b-cell
neutrophil
monocyte
ASPC
endometrium
dendritic cell
macrophage
mesothelium
d
SLIT3
Expression Level
Identity
ASPC
mesothelium
pericyte
adipocyte
macrophage
endothelial
LEC
monocyte
t_cell
dendritic_cell
SMC
b_cell
mast_cell
nk_cell
endometrium
neutrophil
e
Day 0
Day 4
Day 8
SLIT3-FL
SLIT3-N
UCP1
Total Protein

961 **Supplementary Figure 2. Related to Figure 1.**

962 (a–b) UMAP of unsupervised clustering of nuclei from mouse ingWAT and pgWAT (a) and violin
963 plot showing Slit3 transcript expression across clusters (b).

964 (c–d) UMAP of unsupervised clustering of nuclei from human WAT (c) and violin plot showing
965 SLIT3 transcript expression across clusters (d).

966 (e) SLIT3, UCP1, and total protein levels in SVF-derived brown adipocytes at day 0, day 4, and
967 day 8 of differentiation.

968
969
970
971
972
973
974
975
976
977
978
979
980

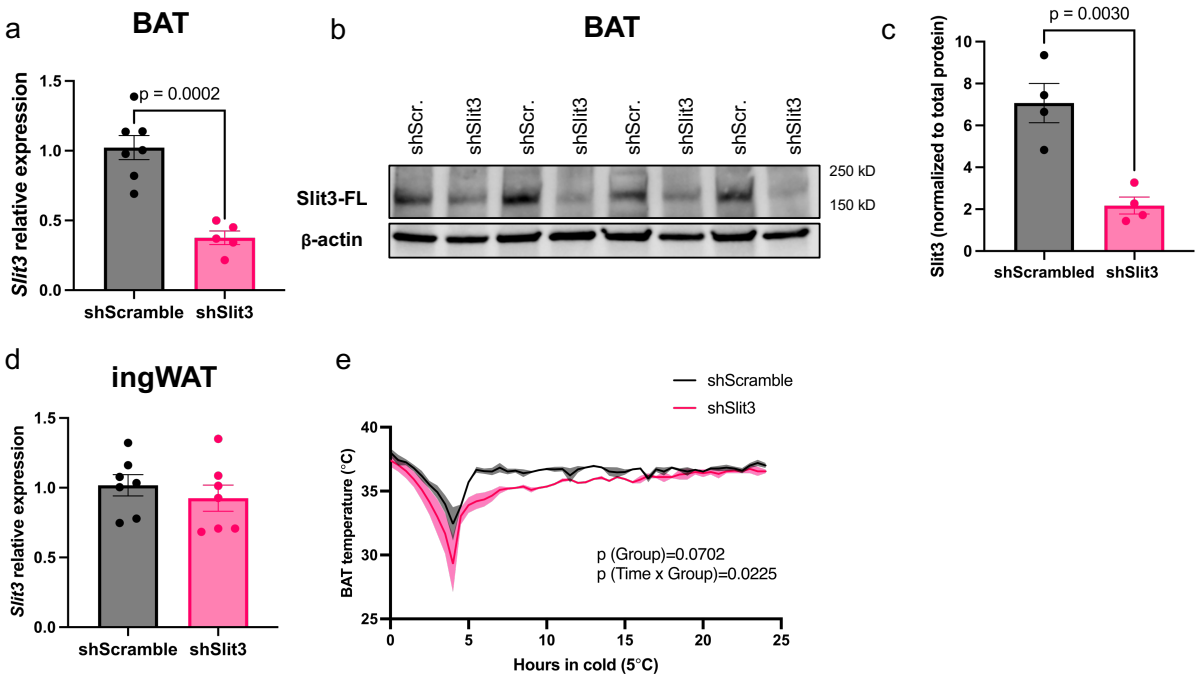

Supplementary Figure 3. Related to Figure 1.

(a) Slit3 transcript levels and (b–c) protein levels in BAT,

(d) Slit3 transcript levels in inguinal WAT (ingWAT), and

(e) BAT temperature in mice injected with AAV-shSlit3 or scramble shRNA and housed at cold (5 °C) for 7 days.

N = 5–7 mice per group. Data are presented as mean ± SEM and analyzed by unpaired two-sided Student's t-tests (a, c) and repeated measures ANOVA (d).

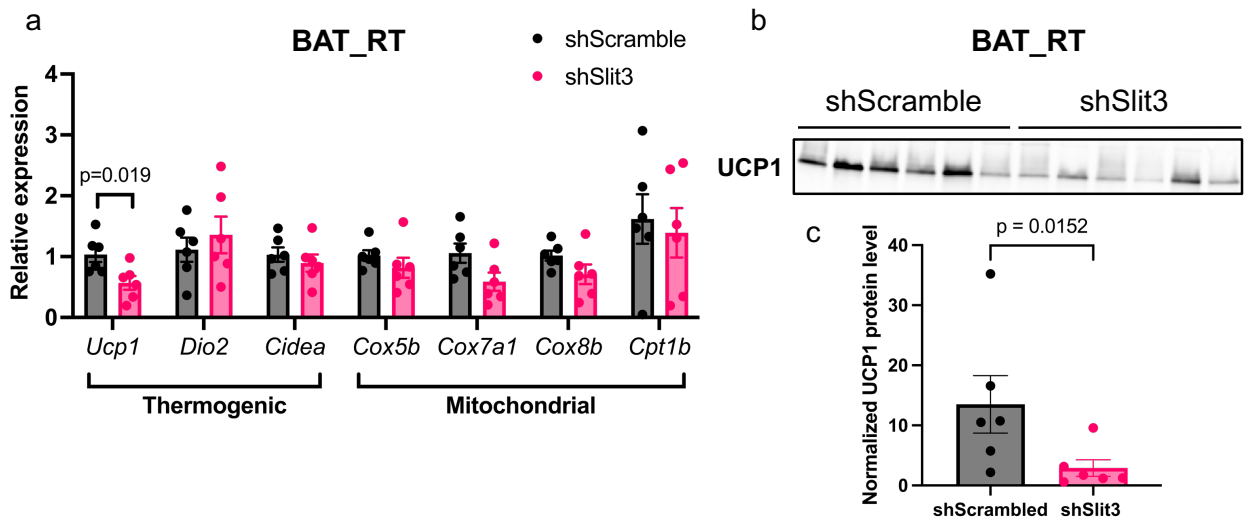

Supplementary Figure 4. Related to Figure 1.

(a) Expression of thermogenic and mitochondrial genes, and (b) UCP1 protein levels in BAT of mice injected with AAV-shSlit3 or scramble shRNA and housed at room temperature. N = 6 per group. Data are presented as mean ± SEM and analyzed by unpaired two-sided Student's t-test (a and c).

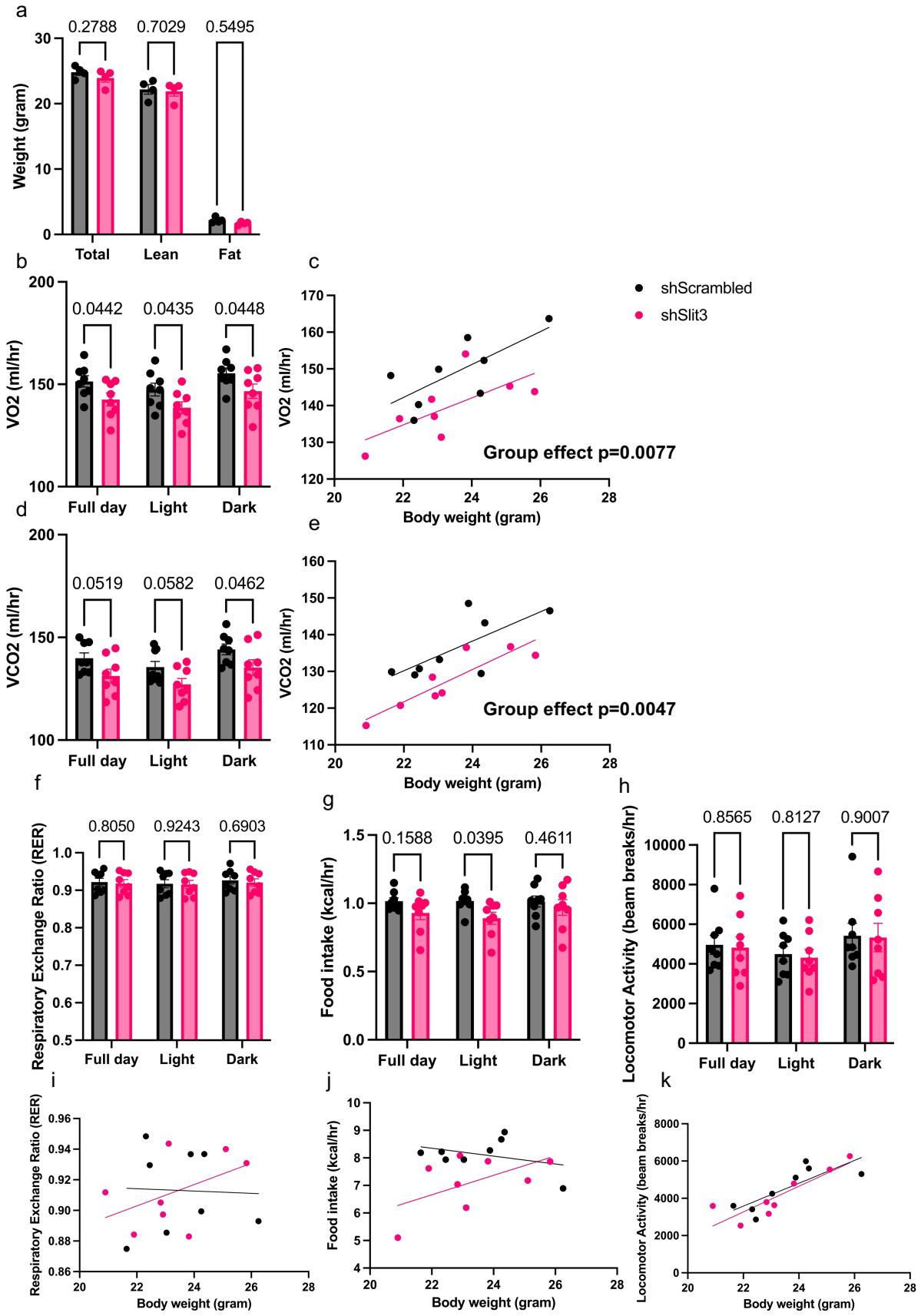
a
0.2788
0.7029
0.5495
Weight (gram)
Total
Lean
Fat
b
0.0442
0.0435
0.0448
VO2 (ml/hr)
Full day
Light
Dark
c
shScrambled
shSlit3
VO2 (ml/hr)
Group effect p=0.0077
Body weight (gram)
d
0.0519
0.0582
0.0462
VCO2 (ml/hr)
Full day
Light
Dark
e
VCO2 (ml/hr)
Group effect p=0.0047
Body weight (gram)
f
0.8050
0.9243
0.6903
Respiratory Exchange Ratio (RER)
Full day
Light
Dark
g
0.1588
0.0395
0.4611
Food intake (kcal/hr)
Full day
Light
Dark
h
0.8565
0.8127
0.9007
Locomotor Activity (beam breaks/hr)
Full day
Light
Dark
i
Respiratory Exchange Ratio (RER)
Body weight (gram)
j
Food intake (kcal/hr)
Body weight (gram)
k
Locomotor Activity (beam breaks/hr)
Body weight (gram)

1007

1008 **Supplementary Figure 5. Related to Figure 1.**

1009 (a) Body composition analysis in mice injected with AAV-shSlit3 or scramble shRNA and housed
1010 at cold (5 °C) for 3 days.

1011 (b, d, f–h) Average hourly rates of VO_2, VCO_2, respiratory exchange ratio (RER), food intake, and
1012 locomotor activity.

1013 (c, e, i–k) Regression plots of VO_2 (c), VCO_2 (e), RER (i), food intake (j), and locomotor activity
1014 (k) versus total body mass.

1015 N = 8 mice per group. Data are presented as mean ± SEM and analyzed by unpaired two-sided
1016 Student's t-test (a), two-way ANOVA (b, d, f–h), and ANCOVA (c, e).

1017

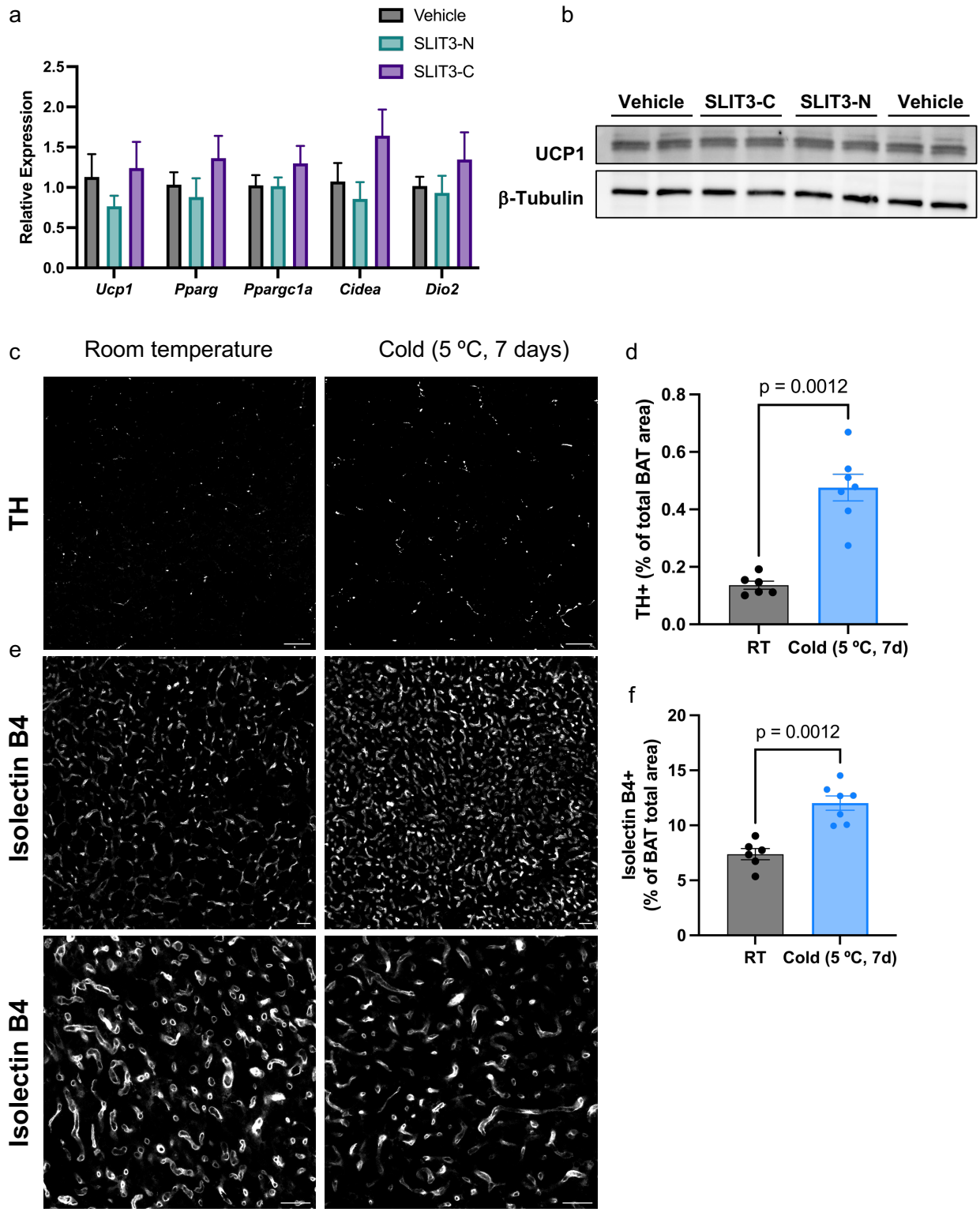

1018

1019

1020

1021 **Supplementary Figure 6. Related to Figure 2.**

1022 (a) Expression of thermogenic genes in in vitro differentiated brown adipocytes treated with
1023 recombinant Slit3-C (100 ng/ml), Slit3-N (100 ng/ml), or vehicle for 48 hours.

1024 (b) UCP1 protein levels in in vitro differentiated brown adipocytes treated with recombinant Slit3-
1025 C, Slit3-N, or vehicle for 48 hours.

1026 (c) Representative images of TH and Plin1 staining and (d) quantification of TH+ neurites per area
1027 in BAT of mice housed at room temperature and cold (5°C) for 7 days. Scale bar = 50 μm.

1028 (e) Representative images of Isolectin B4 staining and (f) quantification of the number of
1029 capillaries per area in BAT housed at room temperature and cold (5°C) for 7 days. Scale bar = 50
1030 μm.

1031 N = 5–7 per group. Data are presented as means ± SEM and analyzed by unpaired two-sided
1032 Student's t-tests (d and f).

1033

1034

1035

1036

1037

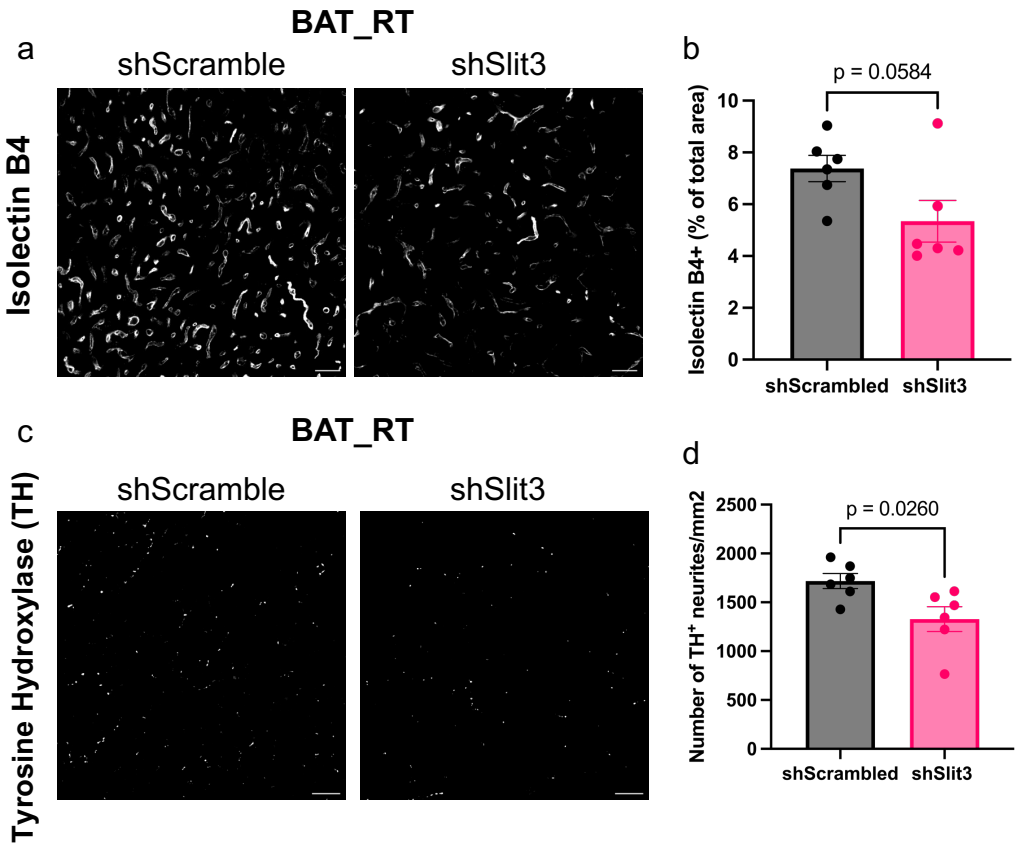

Supplementary Figure 7. Related to Figure 2.

(a) Representative images of Isolectin B4 staining and (b) quantification of the percentage of Isolectin B4+ area in BAT of mice receiving AAV-shSlit3 or scramble shRNA and housed at room temperature. Scale bar = 20 μm.

(c) Representative images of TH staining and (d) quantification of the number of TH+ neurites per area in BAT of mice receiving AAV-shSlit3 or scramble shRNA and housed at room temperature. Scale bar = 25 μm.

N = 6 per group. Data are presented as means ± SEM and analyzed by unpaired two-sided Student's t-tests (b and d)

a **BAT**

Total protein staining for Figure 3a

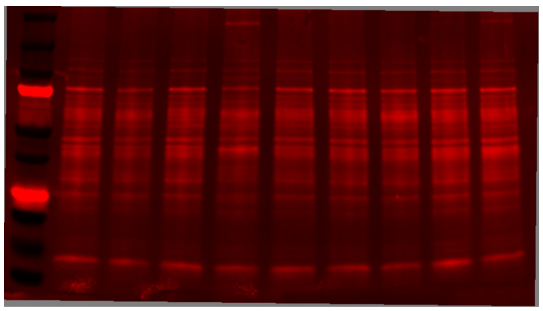

b

Total protein staining for Figure 3C

ingWAT **pgWAT**

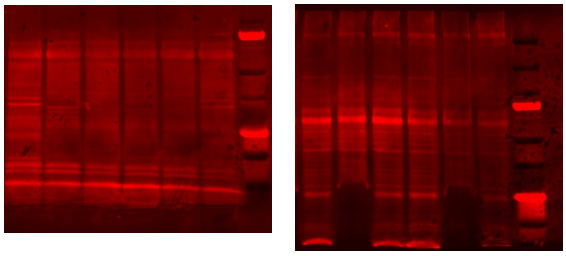

Supplementary Figure 8. Related to Figure 2.

(a-b) Total protein staining corresponding to Figures 3a and 3c.

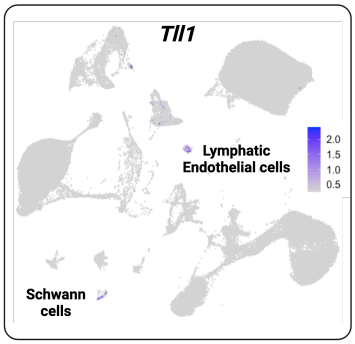

Supplementary Figure 9. Related to Figure 3.

Expression of *Tll1* in scRNA-seq data of mouse BAT.

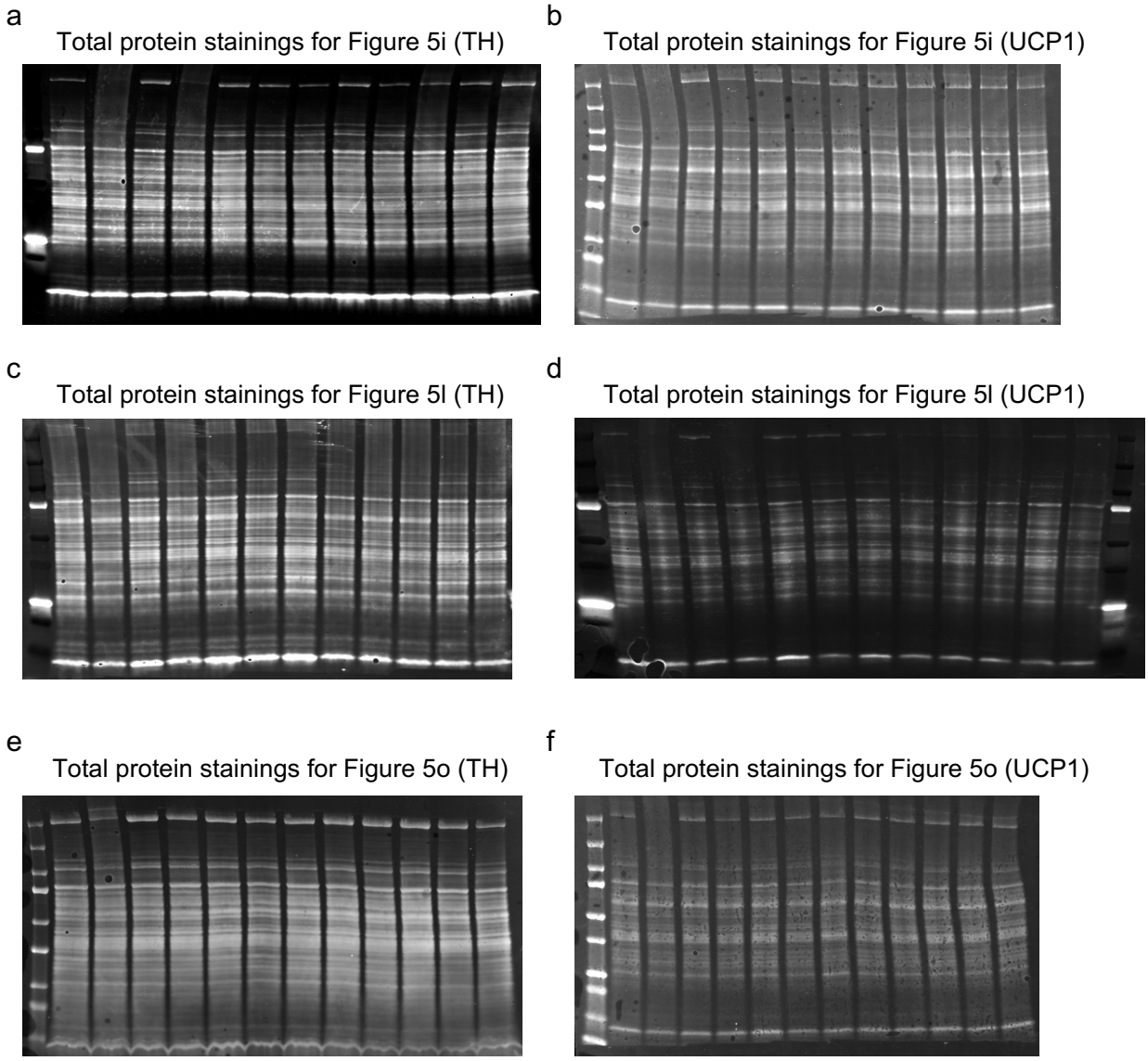

Supplementary Figure 10. Related to Figure 5.

(a–f) Total protein staining corresponding to Figures 5i, 5l, and 5o.

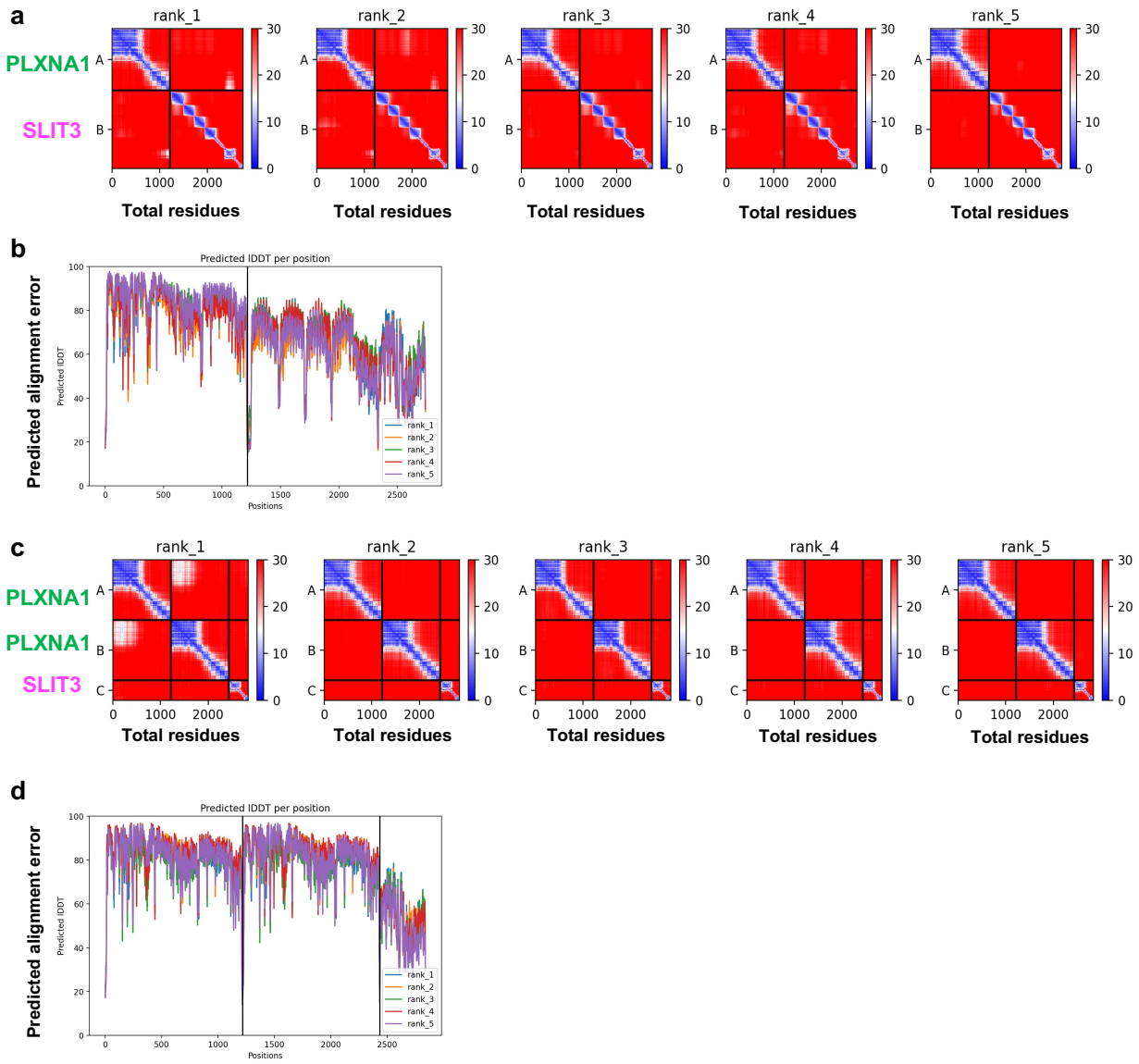

Supplementary Figure 11. Related to Figure 7.

AlphaFold2 Multimer predicts the human PLXNA1-SLIT3 complex. Diagnostic plots and images of 3D models demonstrate the quality of the protein complex predictions using the sequences of human PLXNA1 extracellular domains 1-10 and the C-terminal region of the human SLIT3.

(a) The PAE (predicted error in A° between every pair of residues) plots of monomeric PLXNA1 and SLIT3 interaction model. A and B tiles represent PLXNA1and Slit3, respectively. The X, Y axes indicate the total amino acids in these analyses.

(b) The pLDDT (predicted Local Distance Difference between all atoms) plots show the predicted IDDT per residue in the top five ranked models for monomeric PLXNA1- SLIT3 complex. The X, Y axes indicate the total amino acids in these analyses.

(c) The PAE plot of dimeric PLXNA1 and monomeric SLIT3 interaction model. A and B tiles represent each PLXNA1 monomer, and the C tile shows SLIT3.

(d) The pLDDT plots show the predicted IDDT per residue in the top five ranked models for the PLXNA1 dimer complex with SLIT3.

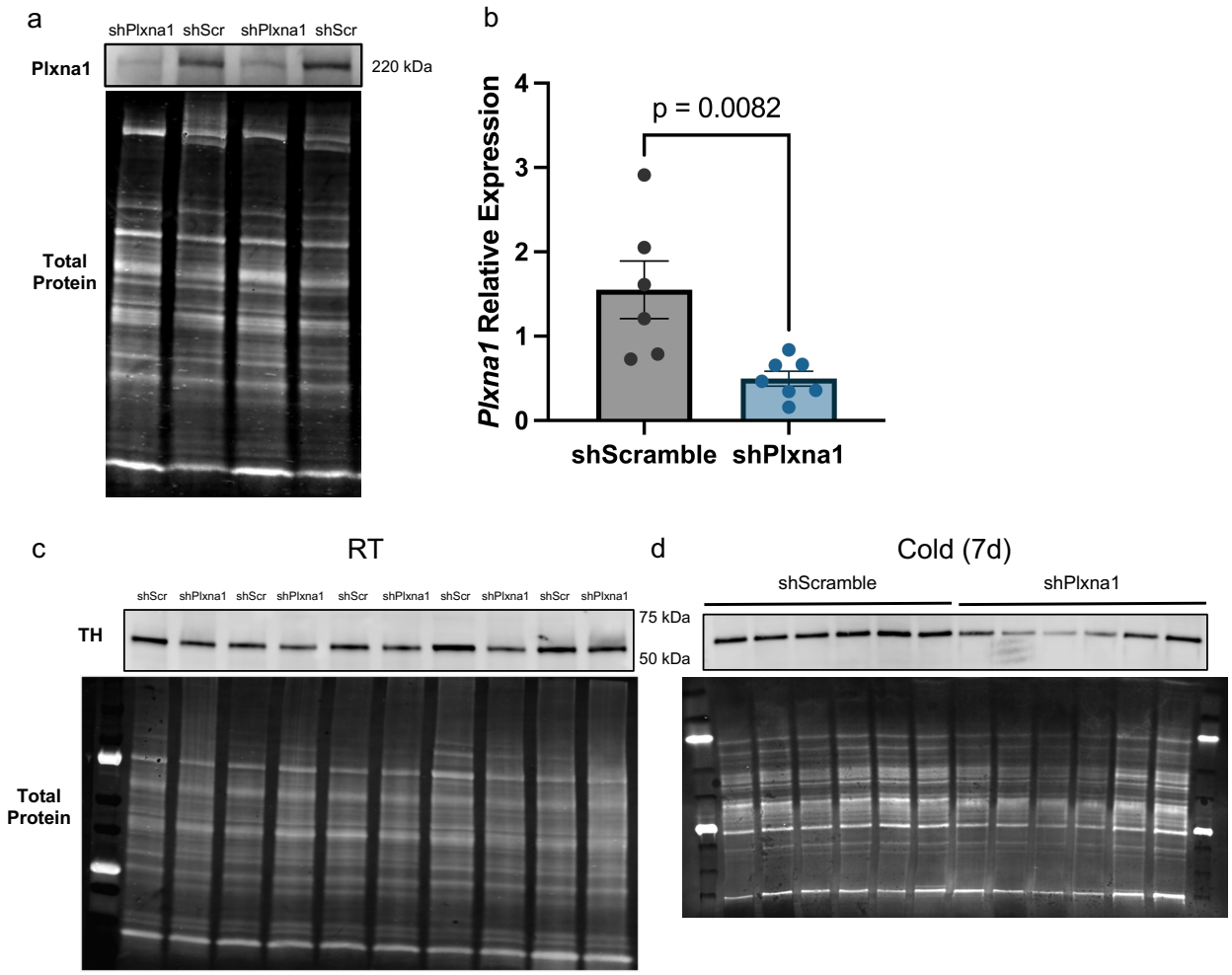

Supplementary Figure 12. Related to Figure 7.

(a) PLXNA1 protein and (b) transcript expression levels.

(c) Total TH protein levels in BAT of mice receiving AAV-shPlxna1 or scramble shRNA.

N = 5 per group. Data are presented as mean ± SEM and analyzed by unpaired two-sided Student's t-test (b).